MESI: A Multiparameter Eddy Significance Index

H.L. Roman-Stork[1,2*], D.A. Byrne[1], and E.W. Leuliette[1]

[1]Lab for Satellite Altimetry, National Oceanic and Atmospheric Administration, College Park, MD, USA. [2]Global Science & Technology, Inc., Greenbelt, MD, USA.

Corresponding author: Heather L. Roman-Stork (heather.roman-stork@noaa.gov)

Key Points:

- A multiparameter index is introduced that estimates the impact of mesoscale eddies on the upper ocean circulation and nutrient cycling
- MESI is most effective when coupled with multiparameter mesoscale eddy tracking
- MESI is shown to be closely related to nutrient values with a cross-correlation of 76-95% in the Northwestern Atlantic Ocean in 2019-2021

Abstract

In this study, we introduce the Multiparameter Eddy Significance Index (MESI) for use in conjunction with mesoscale eddy tracking to estimate the impact of mesoscale eddies on the upper ocean and marine ecosystems. MESI combines blended satellite observations of sea level anomalies (SLA), sea surface temperature (SST), sea surface salinity (SSS), and ocean color chlorophyll-a and is a normalized index. When used in conjunction with mesoscale eddy tracking, MESI can highlight those eddies which extend into the deeper ocean and have a greater effect on nutrient cycling. Preliminary analysis in the Gulf Stream region of the western North Atlantic shows that MESI covaries with model estimates of nitrate, phosphate, iron, and pH with cross-correlation values between 76% and 95%. These results suggest that when MESI is used in concert with eddy tracking, it can be used as an indicator of eddies and areas that are more likely to impact nutrient cycling in the upper ocean. An additional analysis of MESI values inside eddies during Hurricane Dorian (2019) along the Carolina coast further suggests that MESI is most effective when used to enhance eddy tracking as it provides valuable insight into mesoscale eddy activity and the upper ocean circulation.

Plain Language Summary

A Multiparameter Eddy Significance Index (MESI) is introduced in an effort to begin to quantify the potential impact mesoscale eddies have on the upper ocean circulation, nutrient cycling, and biological productivity. The MESI is calculated using satellite observations of sea level anomalies, sea surface temperature and salinity, ocean color derived chlorophyll-a, and eddy kinetic energy and is a normalized index that maintains the integrity of the eddy circulation type. Analysis of MESI values in conjunction with multiparameter mesoscale eddy tracking results for a period from August 2019 - July 2021 suggest that eddies with higher amplitude MESI values penetrate deeper into the upper ocean than eddies with lower amplitude MESI values. In comparing MESI values with nitrate, phosphate, iron, and pH, it was found that MESI covaries with nutrient values with cross-correlations between 76% and 95%, suggesting that MESI can be used as an indicator for nutrient cycling potential within tracked mesoscale eddies. When MESI is paired with eddy tracking, our results suggest that the index can provide valuable insight into eddy activity and impact on the upper ocean, especially during hurricanes and other large storms.

1 Introduction

Mesoscale eddies play a vital role in the global ocean circulation and are critically important for physical, chemical, and biological processes in the ocean. Eddies in the ocean transport physical ocean properties, sediment, and biological matter, such as phytoplankton, fish and coral larvae (Bakun, 2006; Chaigneau et al., 2009; Holland, 1978; McGillicuddy, 2016) and play an important role in nutrient cycling and transport (citations). They also feed back into air-sea interactions and have been known to impact hurricane intensification (Jaimes & Shay, 2009; Kumar & Chakraborty, 2011; Patnaik et al., 2014; Prakash et al., 2021; Sadhuram et al., 2012) and are crucial for ship navigation and fisheries (Arur et al., 2014; Hsu et al., 2015). As such, monitoring and tracking these systems has become a major focus of research (Chaigneau et al.,

2008, 2009; Chanut et al., 2008; Cui et al., 2016; Morrison et al., 2013; Pegliasco et al., 2015; Roman-Stork, Subrahmanyam, & Trott, 2019; Santana et al., 2020).

The physical characteristics and impacts of eddies, particular mesoscale eddies, are reasonably well understood, with studies of the eddy energetics (Cheng et al., 2013; du Toit & Marsden, 2010), air-sea interactions (Morrison et al., 2013; Prakash et al., 2021; Roman-Stork, Subrahmanyam, & Trott, 2019; Trott et al., 2019), and storm implications (Jaimes & Shay, 2009; Kumar & Chakraborty, 2011; Patnaik et al., 2014; Prakash et al., 2021; Sadhuram et al., 2012) becoming increasingly prolific. A recent study has even suggested that ocean eddies are among the major sources of heat transfer to the atmosphere (Su et al., 2018). The timing, placement, circulation, and intensity of eddies are well-known to have influenced the strength and intensity of tropical cyclones (Jaimes & Shay, 2009; Kumar & Chakraborty, 2011; Patnaik et al., 2014; Prakash et al., 2021; Sadhuram et al., 2012), and can even help to determine the timing and strength of Indian Summer Monsoon onset (Neema et al., 2012; Roman-Stork et al., 2020; Shankar et al., 2002; Shenoi et al., 1999). While eddy depth, amplitude, and circulation speed are frequently cited in determining the potential impact of these eddies, often in concert with some measure of sea surface temperature (SST), these parameters are rarely combined with other observations and are often restricted to focusing on eddy energetics while ignoring chemical or biological processes.

Cyclonic eddies (CEs) and Anticyclonic eddies (AEs) are understood to be centers of upwelling and downwelling, respectively, and these physical processes have a major impact on nutrient values and carbon cycling. CEs and cyclonic gyres have been shown to generally have more nutrient-rich, colder waters that support phytoplankton blooms, whereas AEs and anticyclonic gyres tend to have more downwelling processes, warmer waters, and low nutrient values that trend towards oligotrophic conditions and low productivity (Saliglu et al., 1990; others). AEs are not universally oligotrophic, however, and have been shown to have high productivity, in part due to biochemical adaptation and differing nutrient values in the water column (Bibby & Moore, 2010; Johnson et al., 2005; Twining et al., 2009). As such, nutrient cycling in mesoscale eddies has been a major focus of biogeochemical research (Bibby & Moore, 2010; Johnson et al., 2005; Karsetensen et al., 2017; Lee & Williams, 2000; Martin & Pondaven, 2003; McGillicuddy et al., 1998; Nagai et al., 2015; Saliglu et al., 1990; Twining et al., 2009; Xiu et al., 2011; Zhang et al., 2018).

Studies of vertical mixing and nutrient cycling within mesoscale eddies have also highlighted that it is largely the advective processes, not the diffusive processes, which most contribute to nutrient cycling within eddies, and highlight the importance of these structures for phytoplankton blooms and overall net primary productivity (Johnson et al., 2005; Lee & Williams, 2000; Martin & Pondaven, 2003; Nagai et al., 2015; Xiu et al., 2011; Zhang et al., 2018). In regions such as the Sargasso Sea and Gulf Stream, it has been shown that upwelling associated with mesoscale eddies was key for the vertical advection of nitrate into the region and that this nutrient rich water, in combination with replenishment from local nitrification, fueled as much as half of primary production in the region (Martin & Pondaven, 2003; Zhang et al., 2018). Another study in the California Current System found that mesoscale eddies and filaments were major exporters of nitrogen and organic matter from coastal regions into deeper, offshore environments (Nagai et al., 2015). While the role mesoscale eddies play in nutrient cycling may vary globally, overall these structures clearly play a crucial role in both nutrient cycling and determining where net primary productivity occurs.

Due to mesoscale eddies' apparent role in primary productivity and phytoplankton blooms, tracking and monitoring of CEs in conjunction with ocean color observations of chlorophyll-a (Chl-a) is becoming increasingly common, with researchers and fisheries taking advantage of satellite observations to determine where fish are the most likely to be found based on these phytoplankton blooms (Leterme & Pingree, 2008; McGillicuddy, 2016; Park et al., 2020; Pegliasco et al., 2015; Zhang et al., 2019). Eddies are also known to transport harmful algal blooms (Leterme & Pingree, 2008; McGillicuddy, 2016; Santana et al., 2020), coral and fish larvae (Bakun, 2006; McGillicuddy, 2016), and even have impacts on ocean acidification (Hauri et al., 2009). Recently, a number of studies have begun to use eddy tracking to trace the feeding habits of Loggerhead turtles (Gaube et al., 2017; Howell et al., 2010; Kobayashi et al., 2011), melon-headed whales (Woodworth et al., 2011), and other large marine animals (Godø et al., 2012), which are most likely to be found in AEs due convergence and winter mixing (Dufois et al., 2016). By utilizing multiparameter analysis and eddy tracking from satellite observations operationally, these populations can be better monitored, and fisheries can have better guidance in avoiding endangered species, such as Loggerhead turtles.

While there exist many different methods for tracking eddies with varying benefits and limitations (Assassi et al., 2016; Chaigneau et al., 2008, 2009; Chelton et al., 2007; Chelton et al., 2011; Mason et al., 2014; Pegliasco et al., 2015; Yi et al., 2014), there remains a need for a method of simple classification of these systems in terms of physical, chemical, and biological impact on the upper ocean. As a result, a Mesoscale Eddy Significance Index (MESI) is proposed for use in conjunction with operational mesoscale eddy tracking. The MESI combines satellite observations of SST, sea surface salinity (SSS), ocean color Chl-a, eddy kinetic energy (EKE), and sea level anomalies (SLA) and aims to estimate how important and impactful a given eddy can be for upper ocean and surface processes while maintaining the integrity of the eddy circulation.

In this study, eddy tracking was run for 90°W-50°W,10-55°N, the general western North Atlantic and Gulf of Mexico, from August 1, 2019 - July 31, 2021. The paper is structured as follows: the methods and data are presented in sections 2 and 3, the results and associated discussion are presented in section 4; The specific areas of application of MESI in section 4 are as follows: overview and characterization, MESI impact at depth, implications for nutrient cycling, and tropical cyclone interactions with eddies and MESI. Section 5 then summarizes the significance of the findings and concludes the study.

2 Data

2.1 Data used in MESI Calculations

In this study, eddy tracking and surface analysis is performed using global blended multi-mission sea level anomalies (SLAs) and geostrophic currents from the National Oceanic and Atmospheric Administration (NOAA)'s Radar Altimeter Database System (RADS) CoastWatch/OceanWatch near real time (NRT) product (Scharroo et al., 2013). NOAA NRT SLA data is available in a 0.25° horizontal gridded daily product from 2018 to present with geostrophic currents from March 15, 2019 through present. SST data were taken from the L4 NOAA Geo-Polar blended global SST analysis (Maturi et al., 2017). Geo-polar SST data are available on a 1/12° horizontal daily grid from 2019 to present. Ocean color Chl-a data were taken from the NOAA MSL23 Ocean Color NRT VIIRS multi-sensor DINEOF gap-filled analysis (Liu & Wang, 2019). This ocean color product is available in daily format on a 1/12° horizontal grid from 2018

through present. SSS data from the National Aeronautics and Space Administration (NASA)'s Soil Moisture Active Passive (SMAP) version 5.0 Captive Active-Passive product were taken from NASA's Physical Oceanography Distributed Active Archive Center (PO.DAAC) (Entekhabi et al., 2010; Fore et al., 2016). Here the data processed by NASA's Jet Propulsion Lab (JPL) is used in its interpolated daily format (an 8-day running average). This SMAP data product is available from 2015 through present on a 0.25° horizontal grid.

2.2 Satellite Observations for Additional Analysis

Additional satellite observations used in this study include precipitation rate data from the joint NASA/JAXA Global Precipitation Mission (GPM) (Huffman et al., 2019). GPM data is available in a merged product (IMERG) that combines all infrared and microwave observations of precipitation rate from the global meteorology constellation into a single merged product with 0.1° horizontal resolution. Daily NRT GPM data were used in this study and the data are available from 2014 through present via NASA's Earthdata database. Blended surface wind observations were taken from the NRT Cross-Calibrated Multiplatform (CCMP) version 2.1 product (Atlas et al., 2011) published by Remote Sensing Systems (RSS). CCMP combines satellite observations and buoy data overlaid on ERA-Interim fields to estimate 10 m wind values. These data are available in NRT from RSS as a 6-hourly product on a 0.25° horizontal grid from 2015 to present.

2.3 Model Output

Ocean model forecast output from the European Centre for Medium-Range Weather Forecasts (ECMWF)'s Nucleus for the European Modeling of the Ocean (NEMO) version 3.6 obtained from Copernicus Marine Environmental Monitoring Service (CMEMS) are used to supplement observational data at depth (Madec, 2011). NEMO is available as 10-day forecasts in daily temporal resolution with 1/12° horizontal resolution and 50 stratified depths in NRT with a 2-year sliding window from CMEMS. NEMO is principally used as the ocean model component of the ECMWF forecast model but has been used with increased frequency in studies of tropical and subtropical oceans (Momin et al., 2013; Roman-Stork et al., 2019). Additional Operational Mercator Ocean biogeochemical global ocean analysis model output was further obtained from CMEMS (doi 10.48670/moi-00015). This model is forced by NEMOv3.6 and is based on the Pelagic Interactions Scheme for Carbon and Ecosystem Studies (PISCES) biogeochemical model (cite documentation). It is available in a two-year sliding window as a 10-day forecast and is available in 0.25° horizontal resolution with 50 vertical depth layers.

3 Methods

3.1 Eddy Tracking

Eddy tracking is performed using an algorithm originally developed in Chaigneau et al., (2008), Chaigneau et al., (2009), and Pegliasco et al., (2015) that has been optimized for use with NOAA's RADS-based SLA fields and with multiple satellite parameters. This closed-contour eddy tracking method uses daily SLA inputs to track eddy properties and contours using 0.25° horizontal grids and is threshold-free, which allows for smaller, lower amplitude and more transient eddies to be tracked along with the long-term, persistent eddies that are included in other

eddy tracking methods. While frequently filtered out, these transient eddies still play a role in the ocean's circulation and can have a significant impact on air-sea interactions, tropical weather, and even tropical cyclone activity (Greaser et al., 2020; Roman-Stork, Subrahmanyam, & Trott, 2019). While the lack of threshold does mean that some false eddies and filaments are included, some end users may find this information to be of use, and is easily filtered by other end users, so the information is retained.

Valid eddies must contain at least four grid points, which yields a minimum radius of 25 km, meaning that only mesoscale eddies can be tracked with 0.25° data. Eddy trajectories are constructed using a cost function (*CF*):

$$CF_{e_1,e_2} = \sqrt{\left(\frac{\Delta R - \underline{\Delta R}}{\sigma_{\Delta R}}\right)^2 + \left(\frac{\Delta A - \underline{\Delta A}}{\sigma_{\Delta A}}\right)^2 + \left(\frac{\Delta EKE - \underline{\Delta EKE}}{\sigma_{\Delta EKE}}\right)^2} \quad (1)$$

where ΔR, ΔA, and ΔEKE are the differences in eddy radius (R), eddy amplitude (A), and EKE between eddies (e_1, e_2) that intersect (Pegliasco et al., 2015; Roman-Stork, Subrahmanyam, & Trott, 2019), and all average values (ΔR, ΔA, ΔEKE), and standard deviations ($\sigma_{\Delta R}$, $\sigma_{\Delta A}$, $\sigma_{\Delta EKE}$) are determined from the total eddies in the eddy domain. Eddy trajectories are considered valid when eddy tracking is run for a period longer than 100 days, which helps to avoid edge effects and create more accurate contours. In this study, eddy tracking was run for 90°W-50°W,10-55°N from August 1, 2019 - July 31, 2021.

3.2 MESI Construction

The MESI values are calculated using daily satellite data that is regridded onto the SLA grid (0.25° horizontal grid spacing) and normalized to each dataset's own standard deviation. These normalized variables are then multiplied together to achieve the index. EKE values are incorporated into MESI using a $\log_{10}$ scale so as to better match the dynamic range of the other variables. Only the absolute values (*abs*) of all non-SLA variables are utilized so as to maintain the circulation-type of the associated SLA fields, such that all positive MESI values correspond to AEs and all negative MESI values correspond to CEs:

$$MESI = Z_{SLA} * abs(Z_{SST}) * abs(Z_{SSS}) * abs(Z_{Chl-a}) * abs(log_{10}(Z_{EKE})) \quad (2)$$

where $Z_{variable}$ is the normalized value of each variable calculated as in equation 3:

$$Z_{var} = \frac{var - \underline{var}}{\sigma_{var}} \quad (3)$$

where *var* is the variable field, $\underline{var}$ is the unweighted spatial mean of the variable, and σ_{var} is the daily standard deviation. Multiple experimental equations for MESI were tested, but the configuration in Equation 2 was eventually settled upon. This equation, while fairly simple, ensures that the contribution of each variable is felt equally, and if any given eddy is not, for

example, not highly energetic but extremely productive and cold compared to its surroundings, it will still have a higher MESI value. This ensures that no one variable can drown out the contributions of the others.

In constructing the index, maintaining the sign integrity of SLA and including it was decided upon first, along with the inclusion of SST and SSS based on their major contributions to the ocean state and physical processes in the ocean. EKE was included due to its measure of eddy energetics, and a logarithmic measure of it was used so that it would better scale with the other included variables and not overemphasize eddies in regions with high EKE, such as western boundary currents. While not including ocean color Chl-a might have allowed for MESI to remain a strictly physical measure of potential eddy impact, the intention of MESI was to create a biophysical index that had applications for eddy energetics, physical processes, biophysical processes, and biogeochemical processes, and the omission of ocean color Chl-a would have been to its detriment (Figure 1). While the variant that omits SST technically has the highest average correlation with Chl-a (Figure 1g), the physical importance of SST to upper ocean processes necessitated its inclusion. Similarly, while the addition of Ekman pumping (Wek) results in a higher average correlation, the overall spatial response is extremely muted.

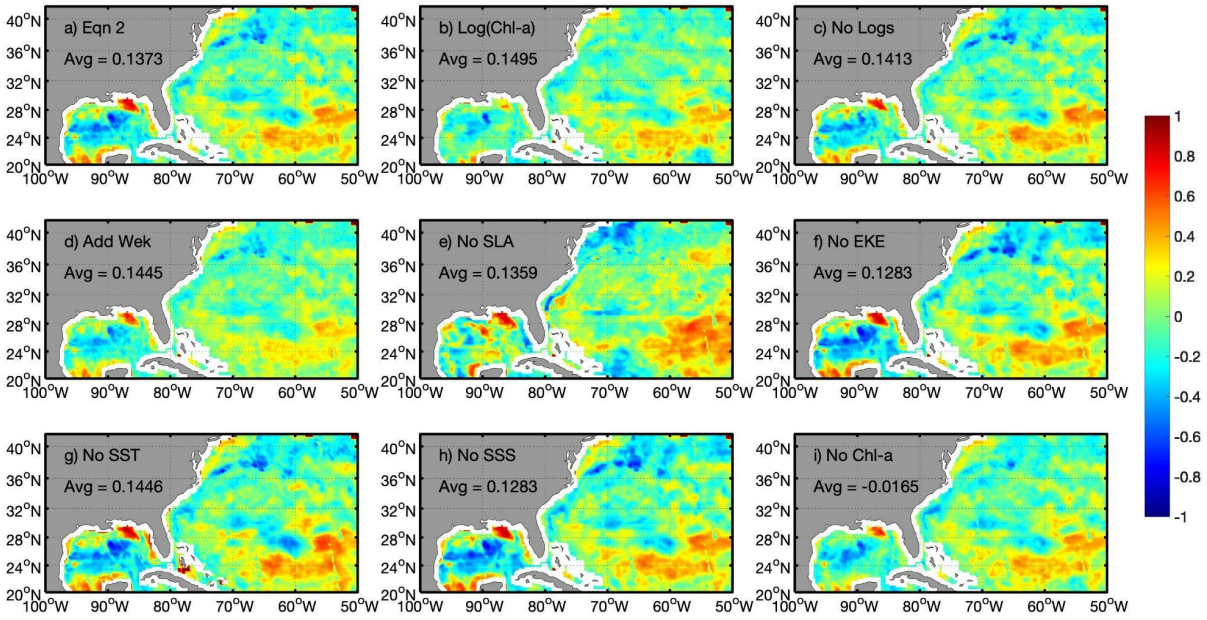

Figure 1. Correlation plots with ocean color Chl-a in the western Atlantic and Gulf of Mexico between August 1, 2019 and July 31, 2021 with the calculated average R^2 values for MESI variants a) Equation 2, b) $\log_{10}$(Chl-a), c) No logarithmic scaling, d) Added Ekman Pumping, e) No SLA, f) no EKE, g) no SST, h) no SSS, and i) no Chl-a.

It should be further noted that the inclusion of variables such as SST and Chl-a from ocean color necessarily involves some manner of cloud contamination. The algorithms used for both products (Maturi et al., 2017; Liu & Wang, 2019) take steps to interpolate and substitute additional observations where satellites cannot directly observe the necessary variable, but the possibility remains regardless and is an inherent part of these types of observations. All observations inherently have some caveats, strengths, and weaknesses associated with them, and

these traits are propagated forward to MESI and measures similar, particularly as MESI incorporates so many different types of observations. It should then be noted that by including these observations, any issues with cloud cover experienced by the products included in the calculation will necessarily be included in MESI. As one of the benefits to our eddy tracking system is that it is threshold free and transient eddies are included, it was important that our MESI configuration was able to highlight transient eddies which had a high apparent impact, even if only briefly. Transient eddies have been shown to have serious impacts on air-sea interactions and monsoon precipitation (Roman-Stork et al., 2019; Greaser et al., 2020), and while different MESI configurations are likely best suited to measuring different impacts of transient eddies on air-sea interactions, upper ocean physical processes, and biophysical processes, we find that the configuration in Equation 2 provides a reasonable estimate and indication of transient eddy impact on these processes (Figure 2, Figure 3). To demonstrate this, radially standardized composites of anticyclones (Figure 2) and cyclones (Figure 3) were created for the transient eddies in the western Atlantic and Gulf of Mexico from August 1, 2019 through July 31, 2021. Without omitting variables from the MESI equation, the configuration in Equation 2 provides the best MESI distribution for the included variables. Compared with the results of ocean color correlation, and by extension biophysical impact (Figure 1), the $\log_{10}$ scaling of ocean color Chl-a weakens the MESI values in both AEs and CEs and not including any logarithmic scaling of EKE muddles the MESI value within the eddy (Figure 2, Figure 3). While the statistical value of the variant without the logarithmic value of EKE appears high, in practice it overemphasized the significance of eddies in high energy regions, such as western boundary currents. Conversely, not including EKE at all removed energetics from the calculation, and our intention is to develop a comprehensive metric.

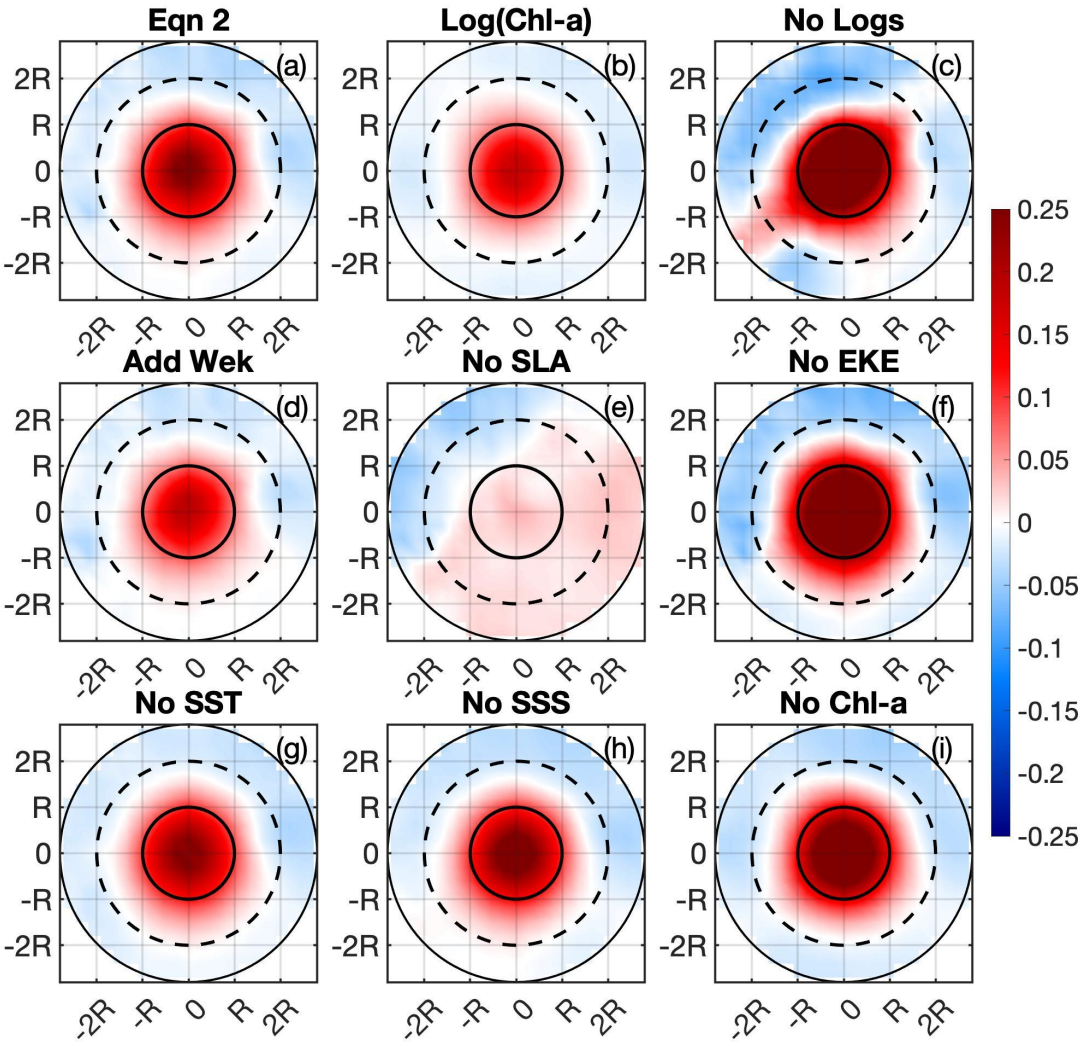

Figure 2. Radially standardized anticyclonic eddy composites in the western Atlantic and Gulf of Mexico from August 1, 2019 through July 31, 2021 for MESI variants a) Equation 2, b) $\log_{10}$(Chl-a), c) No logarithmic scaling, d) Added Ekman Pumping, e) No SLA, f) no EKE, g) no SST, h) no SSS, and i) no Chl-a, where 'R' is taken to be one standardized radius.

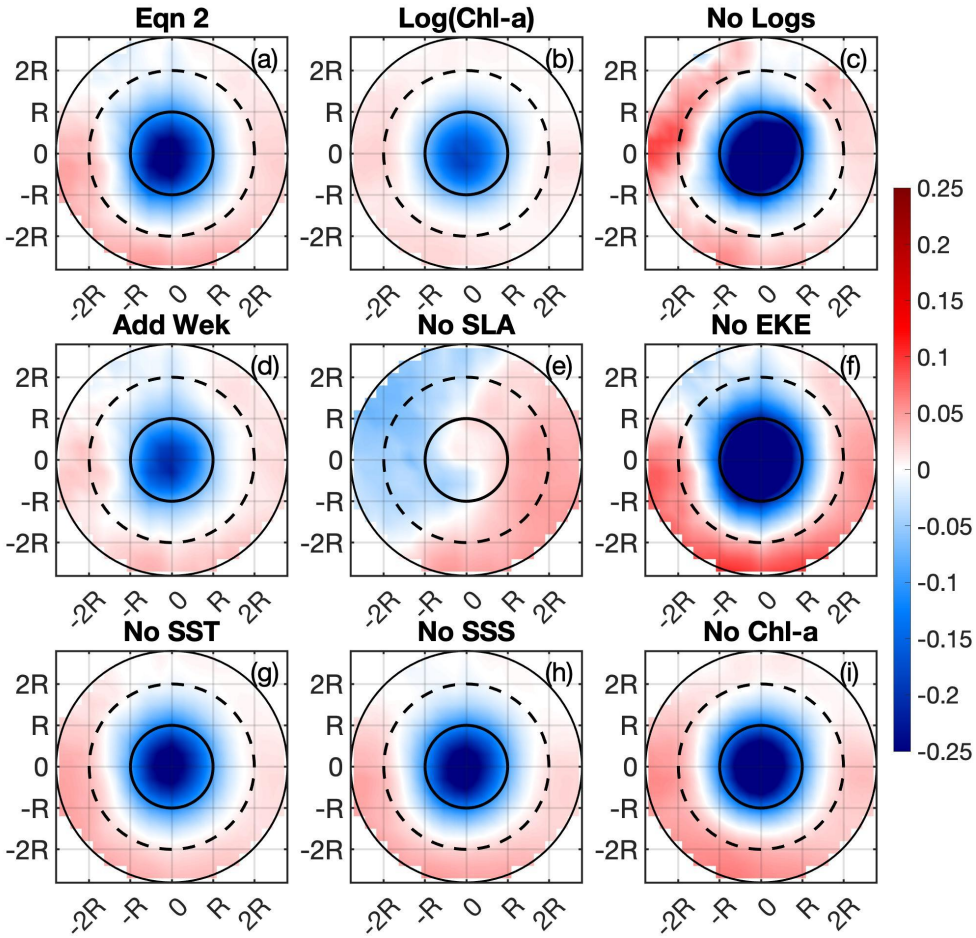

Figure 3. Radially standardized cyclonic eddy composites in the western Atlantic and Gulf of Mexico from August 1, 2019 through July 31, 2021 for MESI variants a) Equation 2, b) $\log_{10}$(Chl-a), c) No logarithmic scaling, d) Added Ekman Pumping, e) No SLA, f) no EKE, g) no SST, h) no SSS, and i) no Chl-a, where 'R' is taken to be one standardized radius.

Finally, in comparing the correlation values of MESI variants with biogeochemical (BGC) variables (iron, nitrate, phosphate, and pH), we find that there was a wide range of performance across variants for each BGC variable (Figure 4). The variants that omitted SST and Chl-a, or had the logarithmic scaled Chl-a performed the worst overall, but other variants omitting SLA, EKE, and SSS appear reasonably well correlated between MESI and BGC variables. The variant that omitted SLA appears to perform surprisingly well, but this performance has been attributed largely to its sign always being positive compared to the other variants, which maintain the sign integrity of the circulation. While this may be the case, the omission of SLA was for the purpose of experimental completion and this variant has no true physical meaning as a metric, given that SLA determines the rotation of the eddy. While certain variants performed exceptionally well for specific BGC variables, Equation 2 came close to matching these correlation values or exceeded them in most cases. Overall, no single variant proved well correlated with every BGC variable, and so MESI should not be considered a 'one-size fits all' index, but rather a general indicator of potential correlation.

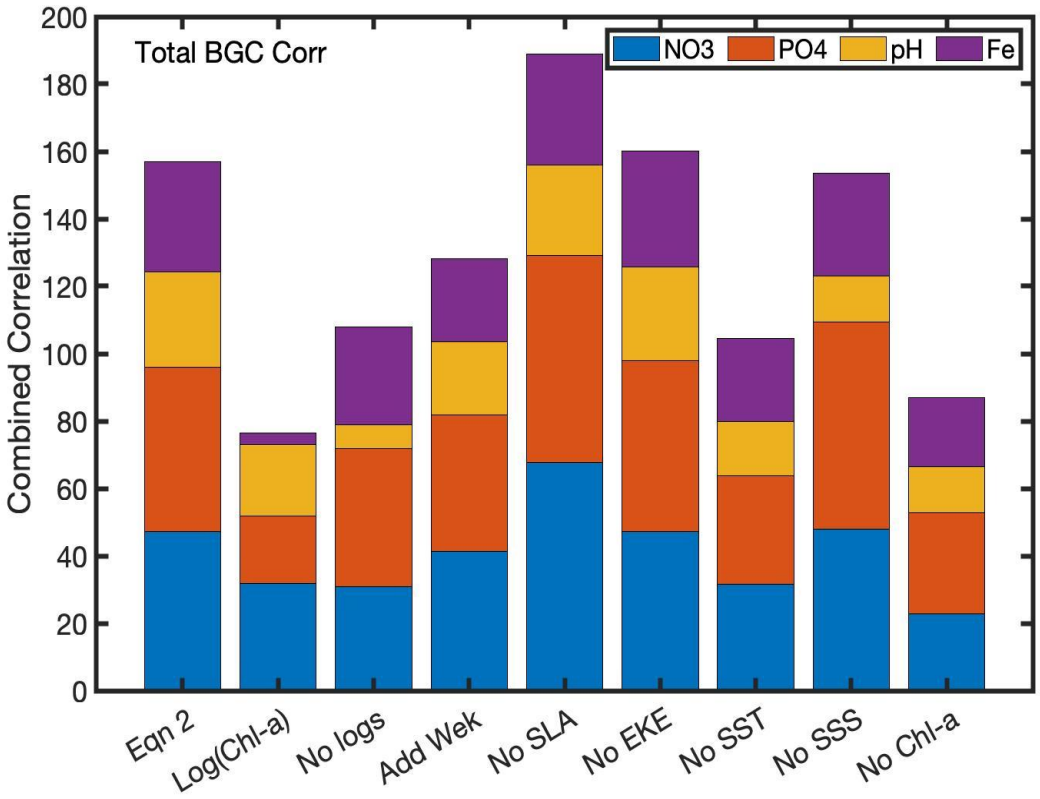

Figure 4. The sum of correlations (corr) for MESI values and biogeochemical (BGC) variables NO_3 (blue), PO_4 (orange), pH (yellow), and Fe (purple) for the entire region of study across all nine MESI variants.

It is likely that no one configuration of MESI is best for all applications and can excel at all available criteria. Of the variants tested, all had their strengths at identifying different variability and differing eddy types. For example, the physical contributions of SST and SSS across eddies are not always uniform dynamically, with some eddies having no clear SST or SSS signal at all, but their physical importance to upper ocean dynamics cannot be ignored, and future iterations of MESI can further explore these complex relationships. It is possible that other configurations not tested can also provide meaningful results, and future iterations can explore regionally variable configurations, but the configuration in Equation 2 has been settled upon for the first iteration of MESI for the reasons previously stated and for the results of our analysis.

4 Results and Discussion

4.1 Overview of the Index

Mesoscale eddies are critically important to the global ocean circulation and the transport of ocean properties, nutrients, biological matter such as coral larvae, and contribute to air-sea interactions and storm intensification (Bakun, 2006; Chaigneau et al., 2009; Holland, 1978; Jaimes & Shay, 2009; Kumar & Chakraborty, 2011; Lee & Williams, 2000; McGillicuddy et al., 1998; McGillicuddy, 2016; Nagai et al., 2015; Patnaik et al., 2014; Prakash et al., 2021; Sadhuram et al., 2012; Salihoglu et al., 1990; Zhang et al., 2018). As such, tracking and characterizing these features can assist in obtaining a more complete picture of interconnected ocean processes.

Satellite observations of SLA, SST, SSS, Chl-a, and derived EKE are combined into the normalized MESI in an attempt to quantify these eddies in multiparameter space and help illuminate, in a simplified representation, their impact on upper ocean biological processes. In this section, we provide an overview of the MESI's characteristics and constituents, explore how deep eddies of varying MESI values penetrate into the upper ocean, and then turn our attention to applications of the MESI in nutrient cycling and hurricane studies.

A direct comparison of constituent variables to MESI values in the Loop Current and Gulf Stream region of the US East Coast overlaid with mesoscale eddy contours demonstrates how the MESI combines the contributions of each variable such that an anomaly in any one variable cannot overwhelm the index (Figure 5). While there are many high amplitude eddies in the sample region (Figure 5f), particularly in the Gulf Stream, this is frequently insufficient to deem the eddies 'impactful' via the index. High impact eddies, indicated by brighter colors in Figure 5a, are most frequently found in near coastal regions, along major currents, and tropical seas. Higher positive MESI values are most frequently found in regions of high EKE and biological productivity, whereas higher negative MESI values are most frequently found in the open ocean, particularly near and around the subtropical gyre. In utilizing the absolute value of contributing variables with the exception of SLA, the integrity of the eddy circulation is maintained, allowing for positive and negative MESI values to be considered in the context of the eddy circulation characteristics, such as for sea turtle feeding patterns (Gaube et al., 2017; Howell et al., 2010; Kobayashi et al., 2011).

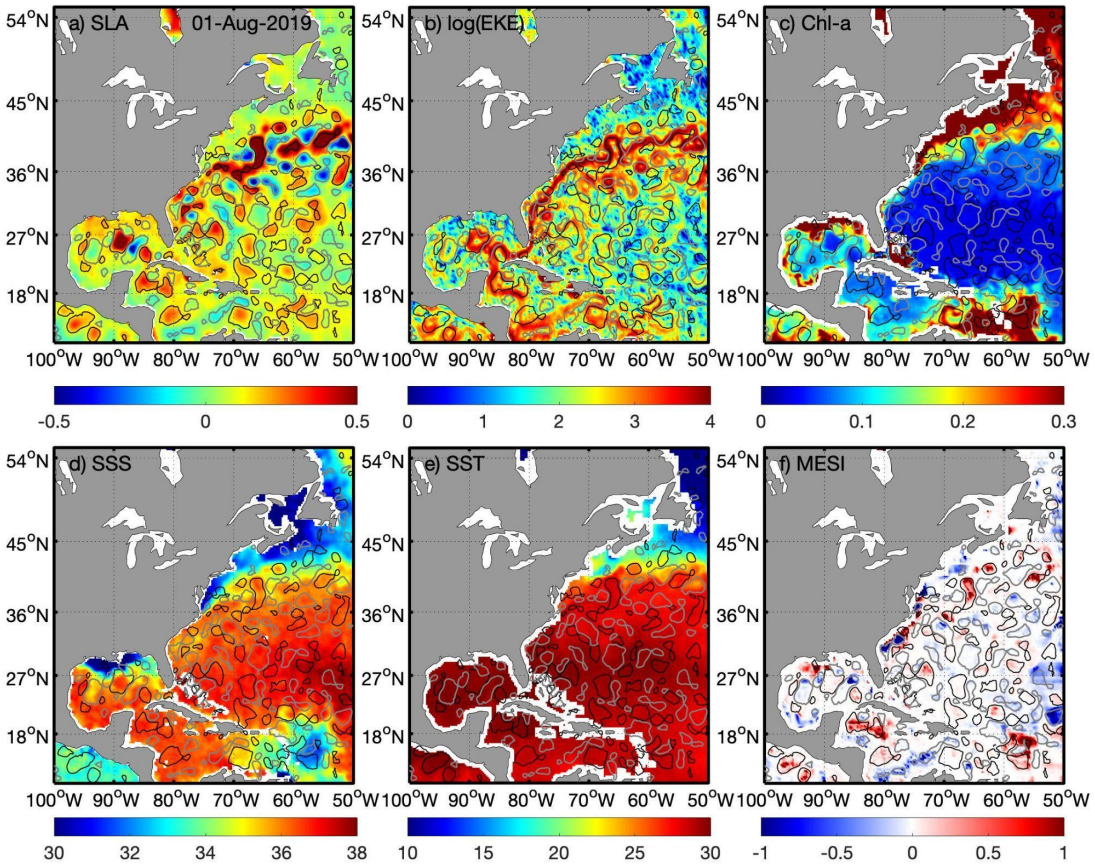

Figure 5. Multivariate satellite observations of (a) NOAA RADS SLA, (b) the $\log_{10}$ of EKE derived from NOAA RADS geostrophic currents (units), (c) Chl-a from ocean color (mg/m^3), (d) SMAP SSS (psu), (e) Geo-polar SST (°C), and (f) calculated MESI in the eastern North Atlantic and US East Coast and Caribbean on August 1, 2019, overlaid with eddy contours for anticyclonic (solid black contours) and cyclonic (gray contours) eddies.

A distribution of MESI values for both AEs and CEs show that both eddy types have a skewed distribution in favor of low MESI values, with the largest spikes being either at or near 0 (Figure 6a). Any overlaps in MESI values of the opposite rotation are likely due to eddies that are very low amplitude and transient, or else false eddies. As shown in Figures 3 and 4, it is also likely that the averaged MESI value shown is not reflective of the circulation type at the center, but rather due to contamination or a secondary circulation. In the region analyzed, CEs tend to have higher amplitude values overall, with the largest overall MESI values being associated with CEs. This is likely due to the tendency of phytoplankton blooms to be associated with upwelling systems, such as those found in CEs, which would naturally skew the index towards higher values for these eddies.

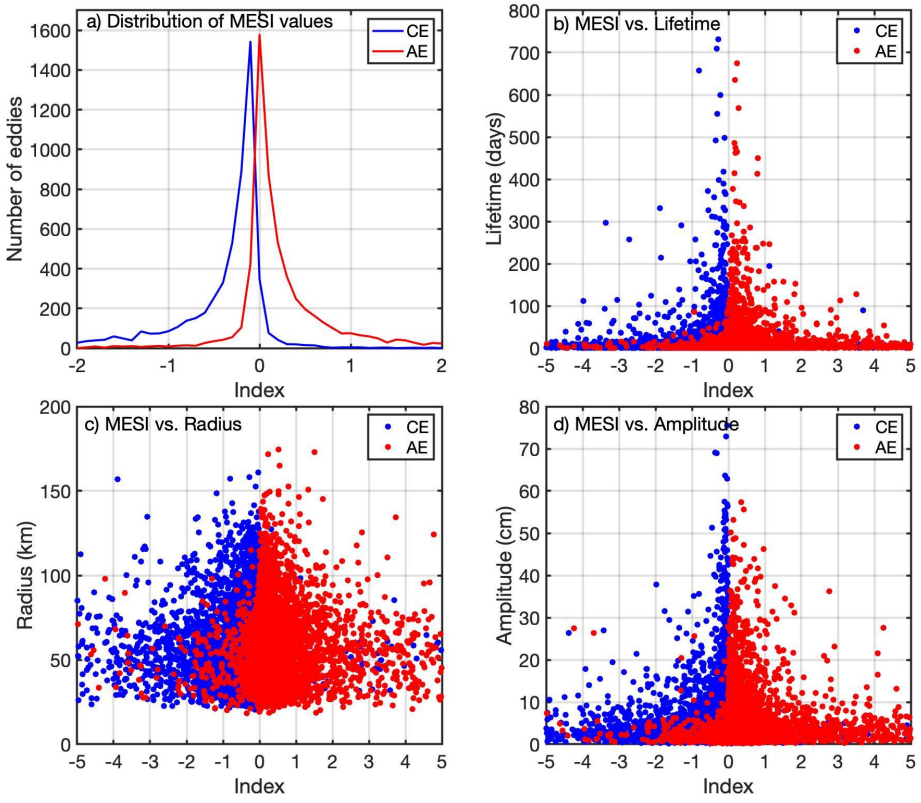

Figure 6. a) Distribution of MESI values in mesoscale cyclonic eddies (CEs; blue) and anticyclonic eddies (AEs; red), and scatter plots of MESI value versus b) eddy lifetime, c) eddy radius, and d) eddy amplitude in the eastern North Atlantic from August 1, 2019 - July 31, 2021.

In comparing MESI values and eddy lifetimes, it becomes clear that more transient eddies frequently have some of the highest MESI values (Figure 6b). Eddies with smaller radii (Figure

6c) and lower amplitudes (Figure 6d) also present a tendency toward higher MESI values than larger, high amplitude eddies. This not only supports the use of a threshold-free eddy tracking methodology, but suggests that smaller eddies, including submesoscale eddies, can still have a major impact on cross-shelf exchange (Brink 2016), mixing (Pegliasco et al., 2015), and air-sea interactions (Su et al., 2018).

4.2 MESI and Depth

To analyze the impact eddies of varying MESI values have on the upper ocean, transects of eddies with a strong negative MESI value (Figure 7), a strong positive MESI value (Figure 8), and three low MESI values (Figure 9) are considered in concert with the multiparameter MESI components.

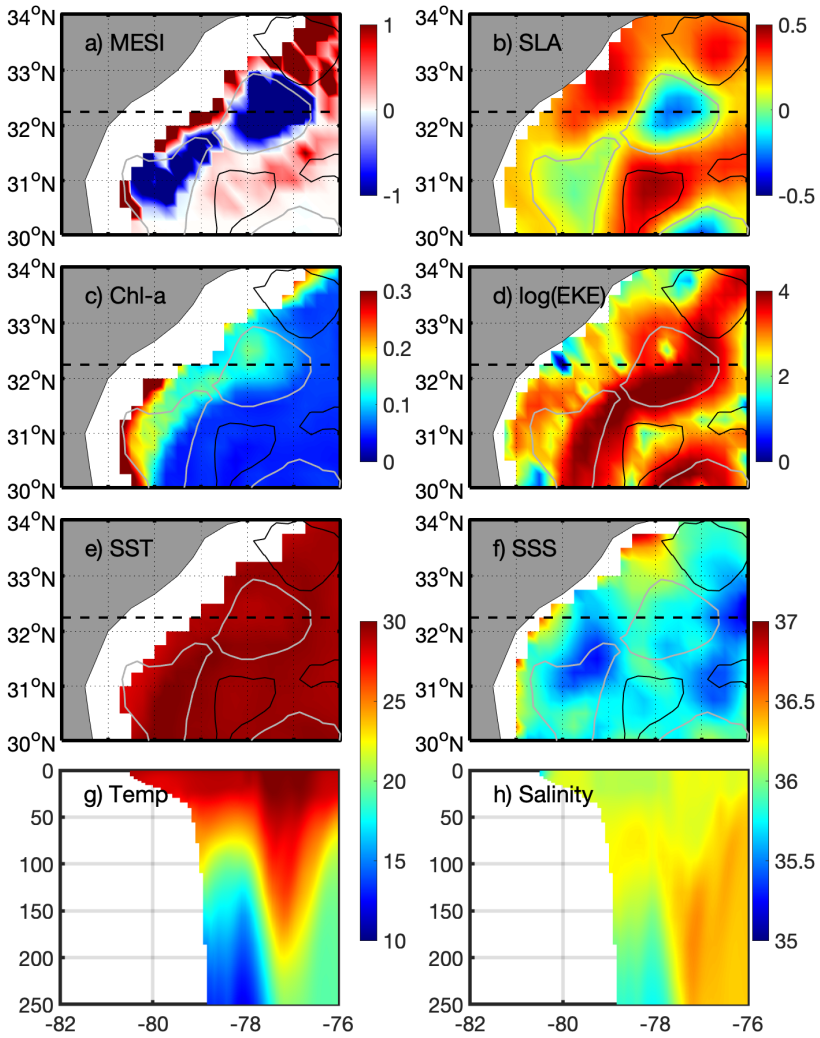

Figure 7. Analysis of an eddy with a strong negative MESI value with surface plots of a) MESI values, b) SLA (m), c) Chl-a (mg/m^3), d) $\log_{10}$ EKE (cm^2/s^2), e) SST (°C), and f) SSS (psu) derived from satellite observations and overlaid with mesoscale eddy contours for anticyclonic

(black contours) and cyclonic (gray contours) eddies and depth transects of g) NEMO model temperature (°C), and h) NEMO model salinity (psu) at the transect in (a-f; dashed black line).

The first sample eddy we consider was found off the US East Coast near Georgia and South Carolina and had an anomalously large negative MESI value (Figure 7). This CE appears reasonably close to the coast, near the limits of coastal processes for several of the satellite data products used. EKE values suggest that this CE was a cold-core Gulf Stream ring, which are known for their high EKE and productivity, (Gangopadhyay et al., 2019; Kang & Curchitser, 2013; Lai & Richardson, 1977; Leterme & Pingree, 2008; Ning et al., 2021). While SLA, EKE, and Chl-a are notably high within this eddy, the SST and SSS values inside the eddy appear largely unremarkable compared to those surrounding it, which is not unusual for a Gulf Stream ring. However, in analyzing this eddy at depth using an ocean model (Figure 7g,h), it can be seen that despite having SST and SSS surface signatures that are similar to those outside of the eddy, subsurface temperatures below 75 m are significantly reduced compared to both the surrounding waters and Gulf Stream, causing a shoaling of the thermocline and pycnocline within the eddy and a huge depression of both in the Gulf Stream that directly borders the eddy. Overall, the high EKE and productivity associated with this eddy, along with its depth and relation to the Gulf Stream, suggest that this eddy would have a strong impact on both the upper ocean and marine ecosystems in the region.

While not Gulf Stream or Loop Current rings, the eddies selected with large positive MESI values in Figure 8 feed into the Loop Current system and have high EKE values associated with them. As is to be expected of most AEs, these eddies have low productivity associated with them, despite their proximity to several coasts, and have high SSTs (~30°C). According to NEMO model output, the leftmost eddy is highly saline, while the rightmost eddy has an eddy center almost 2 psu lower. The relative contributions of the different variables, however, allow for both eddies to have high MESI values at their centers. These eddies also penetrate deep into the upper ocean, with a modeled temperature anomaly to nearly 250 m in the leftmost eddy and a salinity anomaly deeper than 150 m. While this may be in part related to the proximity to the Yucatan Current, shifting the transect north to 20ºN away from the high EKE associated with the current does not depreciate the depth anomalies in temperature or salinity.

In contrast to the high MESI value eddies, the collection of low MESI value eddies presented in Figure 9 do not have a strong impact on the upper ocean. Despite reasonably high amplitudes, the lack of any anomalously high or low values in any of the SST, SSS, Chl-a, or EKE create a low index value for all three eddies. As these eddies are in the open ocean relatively close to the subtropical gyre, lower overall biological activity and fewer fish would be expected in this region. The modeled depth of these eddies is also dramatically less than it is in the high MESI value eddies, with the maximum temperature anomaly occurring at less than 100 m (50 m) depth for the AE (CEs) and salinity being almost uniform with depth for both eddy types. This result suggests that eddies with a high MESI value can indeed have a significant impact on the upper ocean circulation, with strong implications for marine ecosystems, while lower MESI value eddies are less likely to have ecological impact.

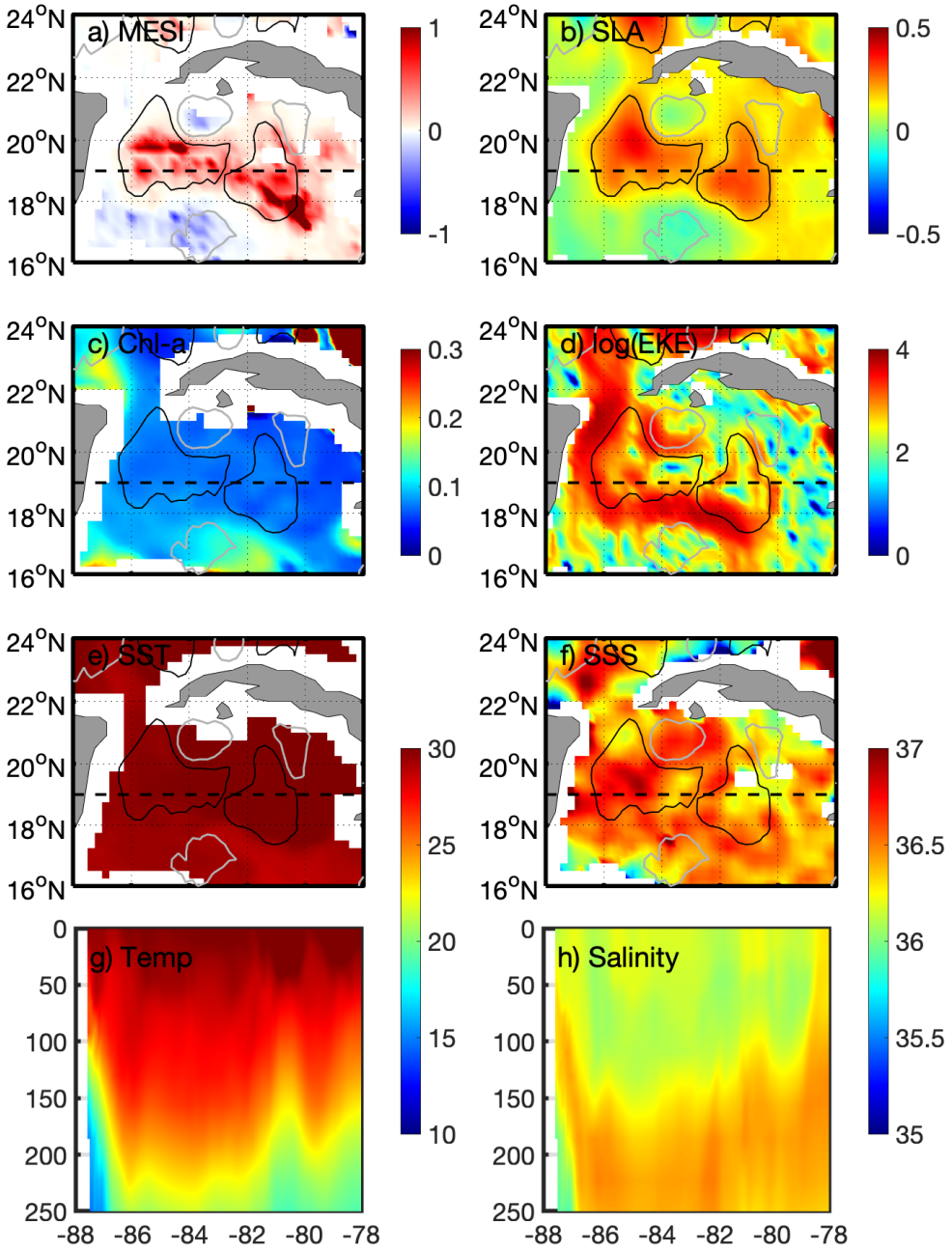

Figure 8. Analysis of an eddy with a strong positive MESI value with surface plots of a) MESI values, b) SLA (m), c) Chl-a (mg/m^3), d) $\log_{10}$ EKE (cm^2/s^2), e) SST (°C), and f) SSS (psu) derived from satellite observations and overlaid with mesoscale eddy contours for anticyclonic (black contours) and cyclonic (gray contours) eddies and depth transects of g) NEMO temperature (°C), and h) NEMO salinity (psu) at the transect in (a-f; dashed black line).

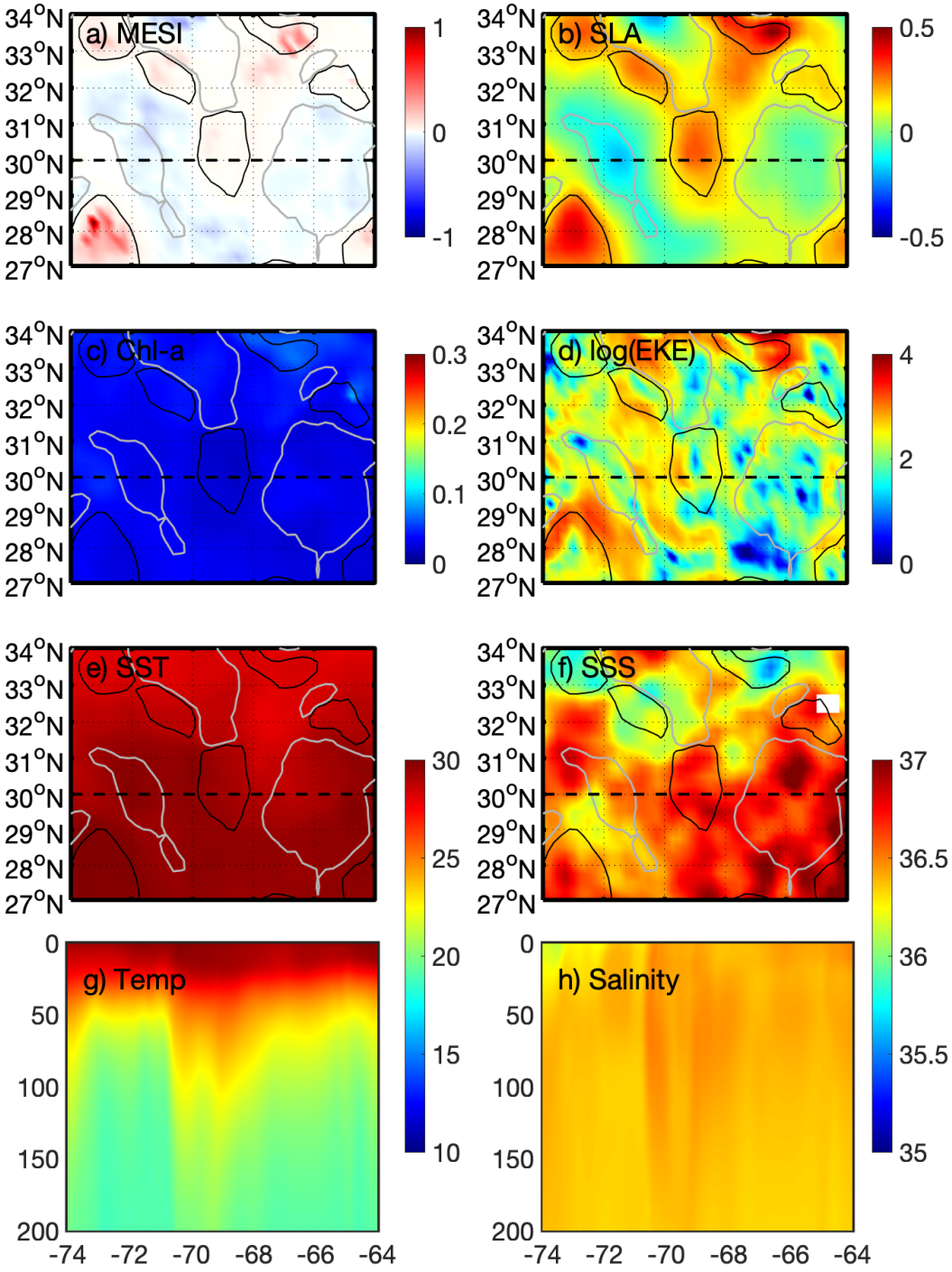

Figure 9. Analysis of three eddies with low MESI values with surface plots of a) MESI values, b) SLA (m), c) Chl-a (mg/m^3), d) $\log_{10}$ EKE (cm^2/s^2), e) SST (°C), and f) SSS (psu) derived from satellite observations and overlaid with mesoscale eddy contours for anticyclonic (black contours) and cyclonic (gray contours) eddies and depth transects of g) NEMO temperature (°C), and h) NEMO salinity (psu) at the transect in (a-f; dashed black line).

4.3 Nutrient Cycling

While it has been shown that eddies with higher MESI values tend to have a greater impact on physical processes in the ocean, we next turn our attention to how MESI values relate to nutrient cycling and chemistry in the upper ocean (Figure 10). Time series of MESI, nitrate, phosphate, iron, and pH (all derived from the CMEMS biogeochemical model output) are compared over the research domain (Figure 10a). For the purpose of clarity, MESI values have been separated into positive and negative values. Nitrate and phosphate exhibit similar behavior, remaining fairly constant through October and then increasing through December. pH, in contrast, increases steadily from August through December, while iron briefly spikes in August, and then steadily decreases over time. While all MESI three time series are more constant than any of the biogeochemical parameters analyzed, the overall trends are nearly inverse with nitrate and phosphate, with the latter seeming to lead trends in MESI. Logically, it follows that an increase in negative MESI values (corresponding to CEs) would correspond to an increase in nutrient values related to upwelling within these systems. This is seemingly supported by the spike in negative MESI values (black dotted line) in Figure 10a in December.

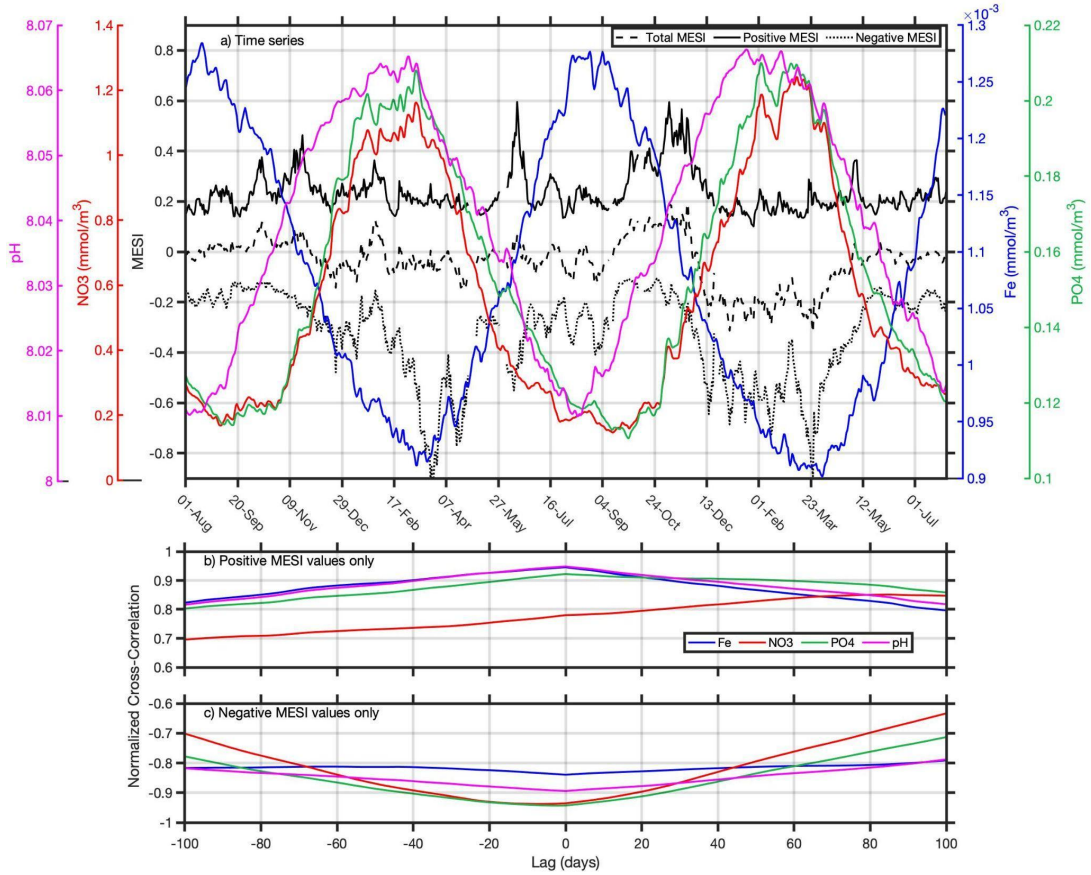

Figure 10. For the entire research domain (90-50°W, 10-55°N) during August 1, 2019-July 31, 2021, a) time series of total MESI (solid black line), positive MESI values only (dashed black line), negative MESI values only (dotted black line), NO_3 (red; mmol/m^3), pH (magenta), Fe (blue; mmol/m^3), and PO_4 (green; mmol/m^3) and b) normalized cross-correlations of NO_3 (red), pH (magenta), Fe (blue), and PO_4 (green) with MESI.

Through calculating the cross-correlation of these biogeochemical variables with positive (Figure 10b) and negative (Figure 10c) MESI values, it can be seen that all four biogeochemical parameters follow a similar overall lead/lag relationship with MESI, save nitrate, which has a lag in AEs. By comparing these variables separately with positive and negative MESI values, it can be seen that there is a strong relationship between biogeochemical processes and MESI values, with iron (95%), phosphate (92%), and pH (95%) exceeding a 90% correlation and nitrate reaching an 85% correlation with 85 days lag for positive MESI values. If only negative MESI values are considered with biogeochemical variables, the variables become anticorrelated given the negative nature of the MESI values (Figure 10b). Negative MESI values have the strongest correlation for nitrate (-94%) and phosphate (-94%), while pH (-89%) and iron (-84%) were substantially lower. Cyclonic eddies, which correspond to negative MESI values, are known to be centers of nutrient pumping in the oceans due to upwelling processes, and the strong correlation between negative MESI values and some biogeochemical variables strongly supports the possibility of using MESI to monitor nutrient cycling in eddies. The use of eddy tracking in concert with MESI values could therefore suggest eddies that are likely to impact nutrient cycling and productivity. As MESI is observational based using satellite data rather than model dependent, its use could allow for an observational proxy for observing biogeochemical variables remotely. The use of longer time series and removal of the seasonal cycles in nutrient values might improve the quantitative correlations and is left for a future, more comprehensive study.

While the majority of experimental analysis has been conducted in the western North Atlantic and Gulf of Mexico, additional biogeochemical analysis in the California Current System (150-100°W, 10-55°N) is conducted for the research period of August 1, 2019 - July 31, 2021. While the dynamics of the California Current System are quite different from the Gulf Stream and neighboring systems, preliminary analysis in this region suggests that MESI remains a powerful tool for biogeochemical analysis in this region (Figure 11).

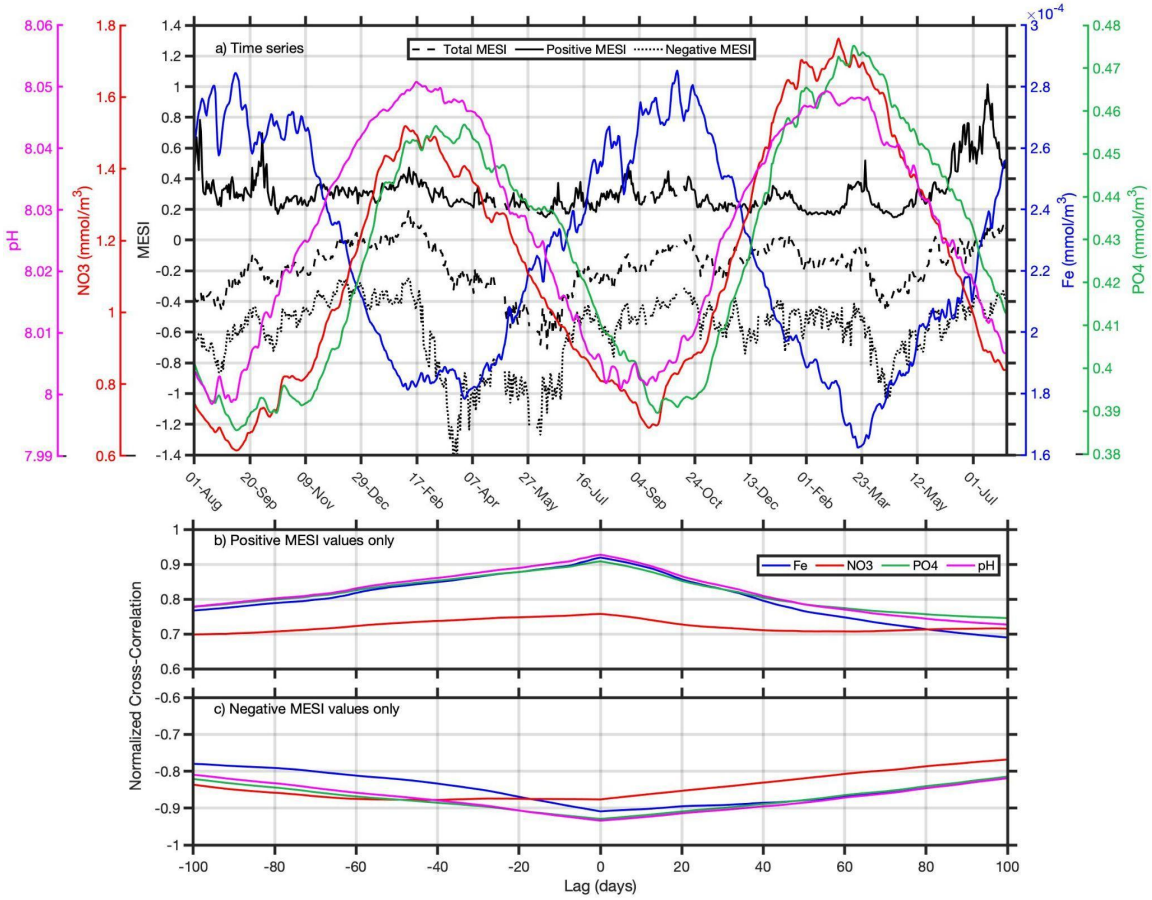

Figure 11. For the California Current System domain (150-100°W, 10-55°N) during August 1, 2019-July 31, 2021, a) time series of total MESI (solid black line), positive MESI values only (dashed black line), negative MESI values only (dotted black line), NO_3 (red; mmol/m^3), pH (magenta), Fe (blue; mmol/m^3), and PO_4 (green; mmol/m^3) and b) normalized cross-correlations of NO_3 (red), pH (magenta), Fe (blue), and PO_4 (green) with MESI.

Seasonal variability and its impact on the relationship between MESI and biogeochemical processes is more pronounced in the California Current System (Figure 11a) than in the western North Atlantic (Figure 10a). This is perhaps best shown in autumn of both years, negative MESI values in the four BGC variables covary in time with negative MESI values, or CEs, a relationship which disintegrates in later months. In winter, MESI also appears to lag the BGC variables, although this is not reflected in the overall cross-correlation, it points to a complex relationship between MESI values and these variables that changes seasonally. As observed in the western North Atlantic in Figure 10, for both positive and negative MESI values, iron, phosphate, and pH exceed a correlation of ±85% at a lag of zero days (Figure 11b, c). The correlation values for nitrate remain lower than the other biogeochemical variables, and as in the western North Atlantic, the correlation for nitrate is higher with negative MESI valued-eddies (-88%) than with positive MESI valued-eddies (76%). While a further, more comprehensive study of the California Current System and its associated eddy variability and biogeochemical processes is surely warranted, our preliminary analysis strongly suggests that the MESI and eddy tracking in this region would be

beneficial for the monitoring of nutrient pumping in this region and further biogeochemical research.

4.4 Implications for Eddy-Cyclone Interactions

Hurricane Dorian (August 26-September 9, 2019) was among the most devastating and powerful Atlantic tropical cyclones in recent memory, with a maximum sustained wind speed of ~82 mph and minimum central pressure of 910 mb (Ezer, 2020). The system formed in the tropical Atlantic before skirting the Caribbean Islands near Cuba, pausing at the Bahamas, and progressing north along the US East Coast before dissipating off the coast of New England (Avila-Alonso et al., 2021; Ezer, 2020; Hazelton et al., 2021). While not infamous for its ocean-eddy interactions such as Rita or Katrina (Jaimes & Shay, 2009), Dorian nonetheless had a significant impact on Gulf Stream volume transport, upper ocean variability along the US East Coast, much of the Sargasso Sea, and other biological productivity in this region (Avila-Alonso et al., 2021; Ezer, 2020; Hazelton et al., 2021).

The impact of Dorian along the southern US coast, from Florida up through South Carolina, can be seen in Figure 12, with rainfall rates from Dorian in excess of 50 mm/day. Its strong winds caused massive amounts of Ekman pumping and upwelling that would later lead to large phytoplankton blooms and significantly reduce the flow of the Gulf Stream (Avila-Alonso et al., 2021; Ezer, 2020). Overlaid with eddy contours, it is clear that only a few strong eddies were present at the peak of the storm, but the data from within these eddies and the total area can still be used to analyze the impact Dorian had on the upper ocean (Figure 12; Figure 13).

We compare time series of MESI, SST, SSS, and Chl-a from within AEs and CEs with the box average of the domain in Figure 12 (82°-72°W, 26°-36°N). Overall, the storm response is found to be highly source dependent, with the data from within the eddies themselves more variable than the box average. Hurricane Dorian passed through this region on September 5-6, 2019, where a peak in MESI values can be seen in all three data sources; however, the box average MESI value peaks at the arrival of the storm, the AE value peaks during the storm, while the MESI values within the CEs drop sharply during the storm. (Figure 13a). Ocean color Chl-a (Figure 13b) proved the greatest difference between AEs and CEs, none of which was apparent in the box average. It is likely that this drop in CE MESI values post-storm is due to the drop in Chl-a preceding it, as well as the upwelling caused by the passage of the storm. In contrast, trends in SSS (Figure 13c) and SST (9d) are similar in all three analysis areas. EKE from within the eddies (Figure 13e) is not dissimilar to Chl-a in the respect that the values within the eddies themselves vary much more widely than the box-averaged values. Given the area of interest, and the work of previous studies regarding Dorian and the Gulf Stream (Ezer, 2020), this is likely a direct response to the storm interacting with the Gulf Stream and propagating this energy into Gulf Stream rings.

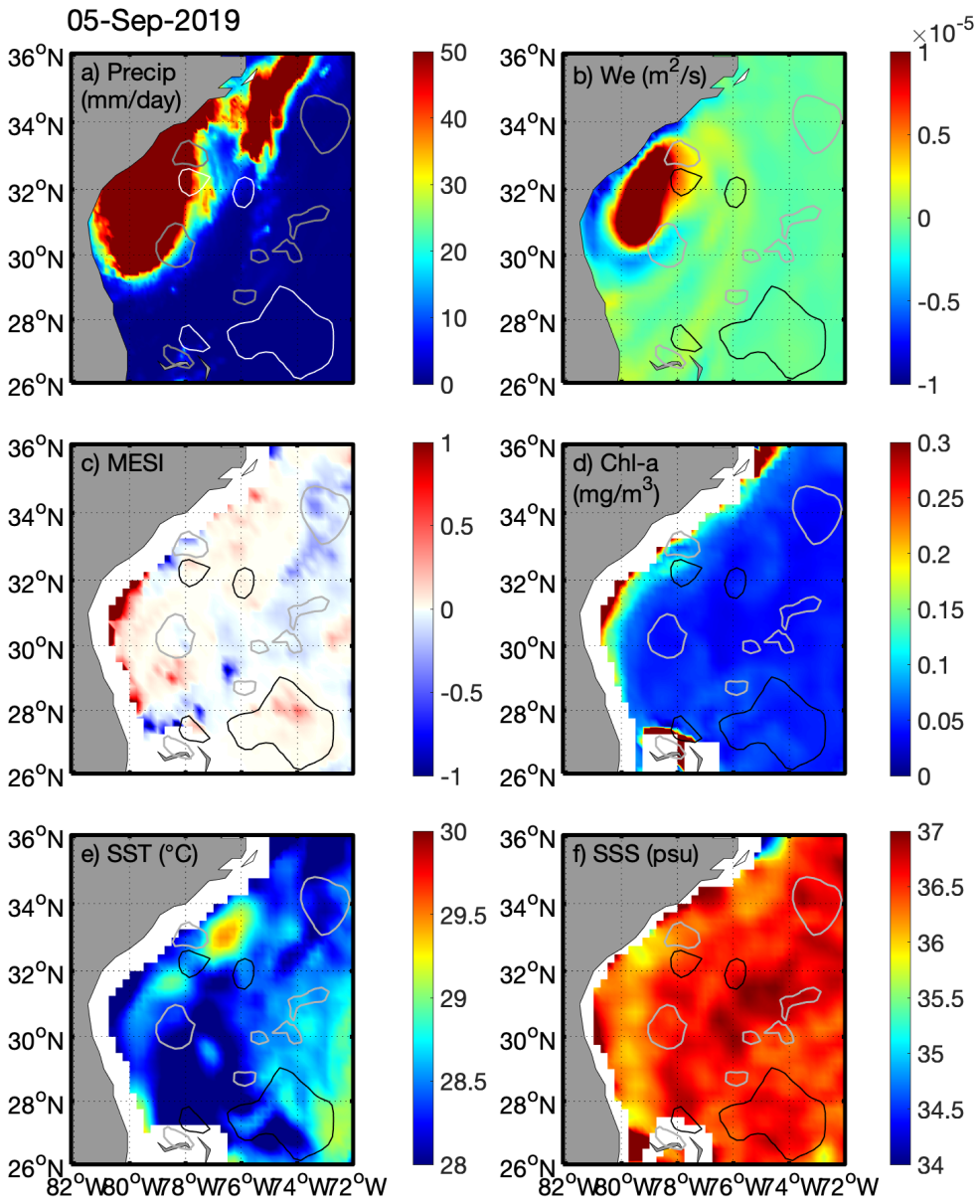

Figure 12. Surface analysis of a) precipitation rate (mm/day), b) Ekman pumping (m^2/s), c) MESI, d) ocean color Chl-a (mg/m^3), e) SST (°C), and f) SSS (psu) off the southern US East Coast on September 5, 2019 during Hurricane Dorian overlaid with mesoscale eddy contours for anticyclonic (solid black/white contours) and cyclonic (gray contours) eddies.

Though the box average will provide a measure of the overall regional response to the storm, the data from within the eddy centers provides a greater insight into some of the extremes experienced by the passage of the storm, particularly with regards to biological productivity. Through our case study of Hurricane Dorian, the benefit of utilizing MESI values in conjunction with eddy tracking becomes apparent; the MESI value reflects the integrated systemic (physical-biological) change to the ecosystem but requires context and the inclusion of additional variables to understand the complete picture. This is perhaps best exemplified in Figure 13, where large

spikes in Chl-a and EKE occur at different times in response to upwelling, winds, and dynamic processes, and thus their individual contributions to MESI are not as clear-cut as when considered alone. However, MESI did spike in both AEs (0.3) and CEs (-0.6) following the passage of the storm, indicating that in conjunction with eddy tracking, the MESI provides a valuable integrated and efficient preliminary qualitative evaluation of eddy productivity and BGC impact.

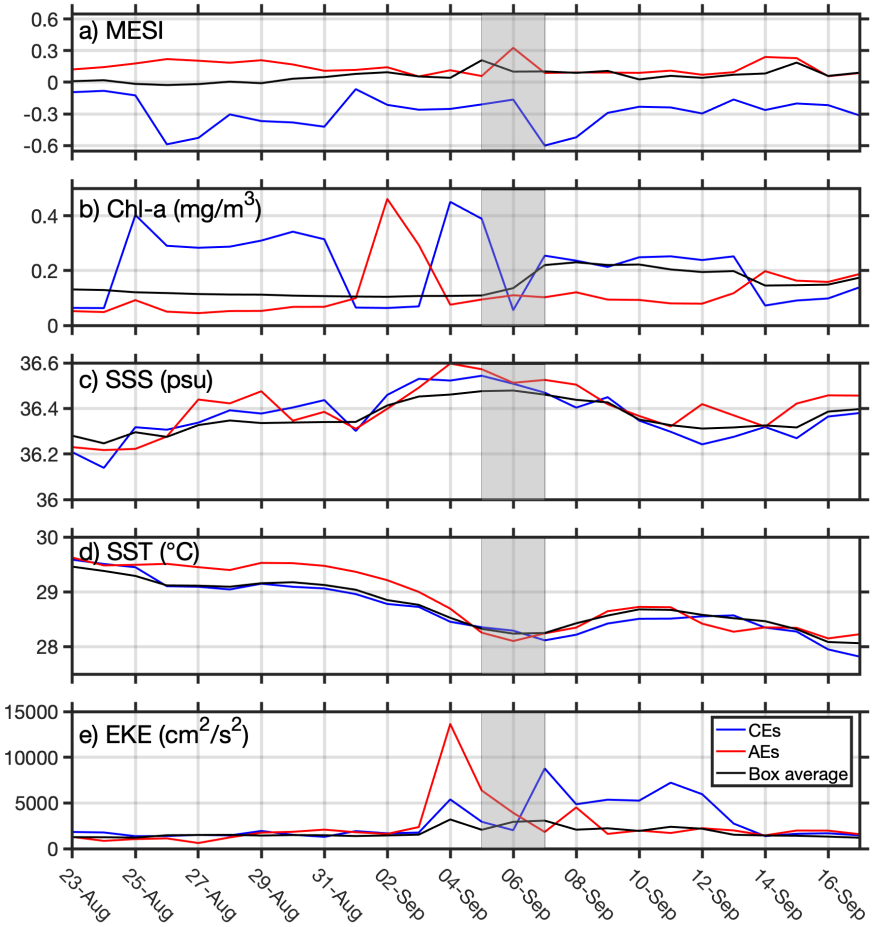

Figure 13. Time series of a) MESI, b) ocean color Chl-a (mg/m^3), c) SSS (psu), d) SST (°C), and EKE (cm^2/s^2) as measured in CEs (blue), AEs, (red) from multiparameter eddy tracking, and a box-averaged in the domain in Figure 11 (82°-72°W, 26°-36°N). Gray shading indicates the passage of Hurricane Dorian (September 5-6, 2019) through this area.

5 Conclusions

In this study, we have introduced MESI, a valuable tool for impact assessment when used in concert with mesoscale eddy tracking. We have shown that even transient eddies can have a major impact on the upper ocean and air-sea interactions, exhibiting high MESI values and potentially high BGC nutrient values and/or productivity even though they are short-lived. In the eddies profiled here, those with higher MESI values tend to penetrate deeper into the upper ocean than those eddies with lower MESI values. Through the inclusion of multiple variables, such as EKE and ocean color Chl-a, we allow for both the eddy's energetics and biophysical impact on upper ocean dynamics to be included when characterizing the eddy, creating a unique integrated

biophysical assessment of an eddy's influence on the ocean with broad applications across oceanographic domains for a wide range of end users. While the possibility of further tuning and improving the MESI in the future remains, the present implementation provides a strong indication of the potential eddy impact on biophysical and biogeochemical processes in mesoscale eddies. The potential applications of MESI are wide and may be used to indicate regions with high megafauna activity, in research of marine ecosystem dynamics, and in studying biophysical responses to synoptic weather events. The idea of MESI in its most basic form is to be a helpful tool and first look indicator that can save the end user the difficulty of pouring through multiple datasets and model outputs and allow them to easily identify areas of potential interest. Even if only used qualitatively, MESI can still prove useful to a wide variety of oceanographic research and operational applications.

Mesoscale eddies are energetic and variable features that play a major role in the global ocean circulation and directly impact the physical, chemical, biological, and geological processes in the ocean. Through the use of the MESI, the integrated impact of these eddies on upper ocean processes can be rapidly estimated. Preliminary analysis of the MESI in conjunction with surface nutrients suggests that the MESI can be used to monitor eddy nutrient values in NRT depending on the region; this capability could prove valuable for nutrient tracing, harmful algal bloom prediction and monitoring, and fisheries management. When used in conjunction with eddy tracking, MESI can also highlight how eddies respond to large-scale ocean-atmosphere coupled events, such as hurricanes, with potential operational and research applications. This index has the advantage of being relatively simple to calculate on the fly in NRT from satellite data or even model output (although this latter formulation has not been tested). When calculated from satellite data, it can provide a strictly observation-based indicator of biogeochemical processes on a large scale within eddies, which are otherwise often difficult to ascertain without a model.

We explored applications of the MESI in two case studies: the seasonal cycle of nutrients in the California Current System, and the effects of Hurricane Dorian in the western North Atlantic. Both cases showed that MESI acts as a succinct summary indicator of biophysical and biogeochemical processes. In comparing the results of these two regions, however, it is clear that the processes that dominate each case are extremely different and therefore so is the relationship between the MESI and the local values of biogeochemical variables. In the western North Atlantic, for example, nitrate had its strongest correlation with MESI at a one-month lag in anticyclonic eddies compared with cyclonic eddies or the eddies in the California Current System. Such case studies will not only help us better understand the physical processes that dominate eddies in each region but, when used in conjunction with eddy tracking, will also help us understand the interplay between physical and biogeochemical processes within eddies and how eddies, in turn, may impact the larger systems in which they are embedded.

Once calibrated for a specific ecosystem, MESI can be used to monitor the biogeochemical processes in the region using satellite observations, rather than relying on (possibly unrealistic) model output, or sparse ship observations. Much as the NINO3.4 index is used to monitor the El Niño Southern Oscillation (ENSO) through an easily obtained, observation-based index, it is our hope that the MESI can be readily used to monitor the impact of mesoscale eddies in a variety of ecosystems and oceanographic processes. Used alongside mesoscale eddy tracking, MESI can be a powerful tool, both operationally and in research, with broad applications across various fields of oceanography.

Acknowledgments

Disclaimer: the scientific results and conclusions, as well as any views or opinions expressed herein, are those of the authors and do not necessarily reflect those of NOAA or the Department of Commerce. The authors declare no conflict of interest.

Funding

Part of this work was performed and funded under ST13301CQ0050/1332KP22FNEED0042.

Open Research

Data Availability

NOAA RADS SLA (Scharroo et al., 2013) and geostrophic currents were found via NOAA CoastWatch and are available in NRT from 2017 through present (SLA) and 2019 through present (currents). The data can be found at https://coastwatch.noaa.gov/cw/satellite-data-products/sea-surface-height/sea-level-anomaly-and-geostrophic-currents-multi-mission-global-optimal-interpolation-gridded.html.

NOAA Geo-Polar SST data (Maturi et al., 2017) was obtained via NOAA CoastWatch and is available from 2019 to present at https://coastwatch.noaa.gov/cw/satellite-data-products/sea-surface-temperature/sea-surface-temperature-near-real-time-geopolar-blended.html. NOAA MSL12 Ocean Color NRT VIIRS multi-sensor Chl-a DINEOF gap-filled data (Liu & Wang, 2019) were obtained from NOAA CoastWatch as a NRT product and are available from 2018 through present via https://coastwatch.noaa.gov/cw/satellite-data-products/ocean-color/near-real-time/viirs-multi-sensor-gap-filled-chlorophyll-dineof.html.

JPL's SMAP SSS Captive Active-Passive V5.0 (Entekhabi et al., 2010; Fore et al., 2016) were obtained from PO.DAAC and are available from 2015 through present via https://podaac-tools.jpl.nasa.gov/drive/files/SalinityDensity/smap/L3/JPL/V5.0/8day_running. The PO.DAAC landing page for SMAP can further be found at: https://podaac.jpl.nasa.gov/dataset/SMAP_JPL_L3_SSS_CAP_8DAY-RUNNINGMEAN_V5?ids=&values=&search=SMAP&provider=PODAAC. CCMP V2.1 surface winds (Atlas et al., 2011) were obtained from RSS and are available in NRT from 2015 through present via https://www.remss.com/measurements/ccmp/. GPM IMERG data (Huffman et al., 2019) are available in NRT from 2014 to present from NASA Earthdata at https://gpm.nasa.gov/data/directory. NEMO forecasts (Madec, 2011) are available in NRT as 10-day forecasts in a 2-year sliding window from CMEMS via https://resources.marine.copernicus.eu/?option=com_csw&view=details&product_id=GLOBAL_ANALYSIS_FORECAST_PHY_001_024. Biogeochemical model data (doi 10.48670/moi-00015) are available in NRT as 10-day forecasts in a 2-year sliding window from CMEMS via https://resources.marine.copernicus.eu/?option=com_csw&view=details&product_id=GLOBAL_ANALYSIS_FORECAST_BIO_001_028. MESIv1 data will be available on NOAA CoastWatch: https://coastwatch.noaa.gov/cwn/index.html.

References

Arur, A., Krishnan, P., George, G., Goutham Bharathi, M. P., Kaliyamoorthy, M., Hareef Baba Shaeb, K., et al. (2014). The influence of mesoscale eddies on a commercial fishery in the

coastal waters of the Andaman and Nicobar Islands, India. *International Journal of Remote Sensing*, *35*(17), 6418–6443. https://doi.org/10.1080/01431161.2014.958246

Assassi, C., Morel, Y., Vandermeirsch, F., Chaigneau, A., Pegliasco, C., Morrow, R., et al. (2016). An Index to Distinguish Surface- and Subsurface-Intensified Vortices from Surface Observations. *Journal of Physical Oceanography*, *46*, 2529–2552. https://doi.org/10.1175/JPO-D-15-0122.1

Atlas, R., Hoffman, R. N., Ardizzone, J., Leidner, S. M., Jusem, J. C., Smith, D. K., & Gombos, D. (2011). A cross-calibrated, multiplatform ocean surface wind velocity product for meteorological and oceanographic applications. *Bulletin of the American Meteorological Society*, *92*(2), 157–174. https://doi.org/10.1175/2010BAMS2946.1

Avila-Alonso, D., Baetens, J. M., Cardenas, R., & De Baets, B. (2021). Oceanic response to the consecutive Hurricanes Dorian and Humberto (2019) in the Sargasso Sea. *Natural Hazards and Earth System Sciences*, *21*(2), 837–859. https://doi.org/10.5194/nhess-21-837-2021

Bakun, A. (2006). Fronts and eddies as key structures in the habitat of marine fish larvae: opportunity, adaptive response and competitive advantage. *Scientia Marina*, *70*(Supl. 2), 105–122. Retrieved from http://www.icm.csic.es/scimar/pdf/70/sm70s2105.pdf

Bibby, T. S., & Moore, C. M. (2011). Silicate: nitrate ratios of upwelled waters control the phytoplankton community sustained by mesoscale eddies in sub-tropical North Atlantic and Pacific. *Biogeosciences*, *8*(3), 657–666. https://doi.org/10.5194/bg-8-657-2011

Brink, K. H. (2016). Cross-Shelf Exchange. *Annual Review of Marine Science*, *8*(1), 59–78. https://doi.org/10.1146/annurev-marine-010814-015717

Chaigneau, A., Gizolme, A., & Grados, C. (2008). Mesoscale eddies off Peru in altimeter records: Identification algorithms and eddy spatio-temporal patterns. *Progress in Oceanography*, *79*(2–4), 106–119. https://doi.org/10.1016/j.pocean.2008.10.013

Chaigneau, A., Eldin, G., & Dewitte, B. (2009). Eddy activity in the four major upwelling systems from satellite altimetry (1992-2007). *Progress in Oceanography*, *83*(1–4), 117–123. https://doi.org/10.1016/j.pocean.2009.07.012

Chelton, D. B., Schlax, M. G., Samelson, R. M., & de Szoeke, R. A. (2007). Global observations of large oceanic eddies. *Geophysical Research Letters*, *34*(15), 1–5. https://doi.org/10.1029/2007GL030812

Chelton, D. B., Schlax, M. G., & Samelson, R. M. (2011). Global observations of nonlinear mesoscale eddies. *Progress in Oceanography*, *91*(2), 167–216. https://doi.org/10.1016/j.pocean.2011.01.002

Chanut, J., Barnier, B., Large, W., Debreu, L., Penduff, T., Molines, J. M., & Mathiot, P. (2008). Mesoscale Eddies in the Labrador Sea and Their Contribution to Convection and Restratification. *Journal of Physical Oceanography*, *38*(8), 1617–1643. https://doi.org/10.1175/2008JPO3485.1

Cheng, X., Xie, S. P., McCreary, J. P., Qi, Y., & Du, Y. (2013). Intraseasonal variability of sea surface height in the Bay of Bengal. *Journal of Geophysical Research: Oceans*, *118*(2), 816–830. https://doi.org/10.1002/jgrc.20075

Cui, W., Yang, J., & Ma, Y. (2016). A statistical analysis of mesoscale eddies in the Bay of Bengal from 22–year altimetry data. *Acta Oceanologica Sinica*, *35*(11), 16–27. https://doi.org/10.1007/s13131-016-0945-3

Dufois, F., Hardman-Mountford, N. J., Greenwood, J., Richardson, A. J., Feng, M., & Matear, R. J. (2016). Anticyclonic eddies are more productive than cyclonic eddies in subtropical gyres because of winter mixing. *Science Advances*, *2*(5), 1–7.

https://doi.org/10.1126/sciadv.1600282
Entekhabi, D., Njoku, E. G., O'Neill, P. E., Kellogg, K. H., Crow, W. T., Edelstein, W. N., et al. (2010). The soil moisture active passive (SMAP) mission. *Proceedings of the IEEE*, *98*(5), 704–716. https://doi.org/10.1109/JPROC.2010.2043918
Ezer, T. (2020). The long-term and far-reaching impact of hurricane Dorian (2019) on the Gulf Stream and the coast. *Journal of Marine Systems*, *208*(2019). https://doi.org/10.1016/j.jmarsys.2020.103370
Fore, A. G., Yueh, S. H., Tang, W., Stiles, B. W., & Hayashi, A. K. (2016). Combined Active/Passive Retrievals of Ocean Vector Wind and Sea Surface Salinity With SMAP. IEEE Transactions on Geoscience and Remote Sensing, 54(12), 7396–7404. https://doi.org/10.1109/TGRS.2016.2601486
Gangopadhyay, A., Gawarkiewicz, G., Silva, E. N. S., Monim, M., & Clark, J. (2019). An Observed Regime Shift in the Formation of Warm Core Rings from the Gulf Stream. *Scientific Reports*, *9*(1), 1–9. https://doi.org/10.1038/s41598-019-48661-9
Gaube, P., Barceló, C., McGillicuddy, D. J., Domingo, A., Miller, P., Giffoni, B., et al. (2017). The use of mesoscale eddies by juvenile loggerhead sea turtles (Caretta caretta) in the southwestern Atlantic. *PLoS ONE*, *12*(3). https://doi.org/10.1371/journal.pone.0172839
Godø, O. R., Samuelsen, A., Macaulay, G. J., Patel, R., Hjøllo, S. S., Horne, J., et al. (2012). Mesoscale eddies are oases for higher trophic marine life. *PLoS ONE*, *7*(1), 1–9. https://doi.org/10.1371/journal.pone.0030161
Greaser, S. R., Subrahmanyam, B., Trott, C. B., & Roman-Stork, H. L. (2020). Interactions Between Mesoscale Eddies and Synoptic Oscillations in the Bay of Bengal During the Strong Monsoon of 2019. *Journal of Geophysical Research: Oceans*, *125*(10), 1–29. https://doi.org/10.1029/2020JC016772
Hauri, C., Gruber, N., Plattner, G. K., Alin, S., Feely, R. A., Hales, B., & Wheeler, P. A. (2009). Ocean acidification in the California current system. *Oceanography*. https://doi.org/10.5670/oceanog.2009.97
Hazelton, A., Alaka, G. J., Cowan, L., Fischer, M., & Gopalakrishnan, S. (2021). Understanding the processes causing the early intensification of hurricane dorian through an ensemble of the hurricane analysis and forecast system (Hafs). *Atmosphere*, *12*(1), 1. https://doi.org/10.3390/atmos12010093
Holland, W. R. (1978). The Role of Mesoscale Eddies in the General Circulation of the Ocean--Numerical Experiments Using a Wind-Driven Quasi-Geostrophic Model. *Journal of Physical Oceanography*, *8*(3), 363–392. https://doi.org/https://doi.org/10.1175/1520-0485(1978)008<0363:TROMEI>2.0.CO;2
Howell, E. A., Dutton, P. H., Polovina, J. J., Bailey, H., Parker, D. M., & Balazs, G. H. (2010). Oceanographic influences on the dive behavior of juvenile loggerhead turtles (Caretta caretta) in the North Pacific Ocean. *Marine Biology*, *157*(5), 1011–1026. https://doi.org/10.1007/s00227-009-1381-0
Hsu, A. C., Boustany, A. M., Roberts, J. J., Chang, J. H., & Halpin, P. N. (2015). Tuna and swordfish catch in the U.S. northwest Atlantic longline fishery in relation to mesoscale eddies. *Fisheries Oceanography*, *24*(6), 508–520. https://doi.org/10.1111/fog.12125
Huffman, G. J., Bolvin, D. T., Braithwaite, D., Hsu, K.-L., Joyce, R. J., Kidd, C., et al. (2019). Integrated Multi-satellite Retrievals for the Global Precipitation Measurement (GPM) Mission (IMERG), (March), 343–353. https://doi.org/10.1007/978-3-030-24568-9_19
Jaimes, B., & Shay, L. K. (2009). Mixed layer cooling in mesoscale oceanic eddies during

Hurricanes Katrina and Rita. *Monthly Weather Review*, *137*(12), 4188–4207. https://doi.org/10.1175/2009MWR2849.1

Kang, D., & Curchitser, E. N. (2013). Gulf Stream eddy characteristics in a high-resolution ocean model. *Journal of Geophysical Research: Oceans*, *118*(9), 4474–4487. https://doi.org/10.1002/jgrc.20318

Karstensen, J., Schütte, F., Pietri, A., Krahmann, G., Fiedler, B., Grundle, D., et al. (2017). Upwelling and isolation in oxygen-depleted anticyclonic modewater eddies and implications for nitrate cycling. *Biogeosciences*, *14*(8), 2167–2181. https://doi.org/10.5194/bg-14-2167-2017

Kobayashi, D. R., Cheng, I. J., Parker, D. M., Polovina, J. J., Kamezaki, N., & Balazs, G. H. (2011). Loggerhead turtle (Caretta caretta) movement off the coast of Taiwan: Characterization of a hotspot in the East China Sea and investigation of mesoscale eddies. *ICES Journal of Marine Science*, *68*(4), 707–718. https://doi.org/10.1093/icesjms/fsq185

Kumar, B., & Chakraborty, A. (2011). Movement of seasonal eddies and its relation with cyclonic heat potential and cyclogenesis points in the Bay of Bengal. *Natural Hazards*, *59*(3), 1671–1689. https://doi.org/10.1007/s11069-011-9858-9

Lai, D. Y., & Richardson, P. L. (1977). Distribution and Movement of Gulf Stream Rings. *Journal of Physical Oceanography*, *7*(5), 670–683.

Leterme, S. C., & Pingree, R. D. (2008). The Gulf Stream, rings and North Atlantic eddy structures from remote sensing (Altimeter and SeaWiFS). *Journal of Marine Systems*, *69*(3–4), 177–190. https://doi.org/10.1016/j.jmarsys.2005.11.022

Liu, X., & Wang, M. (2019). Filling the gaps of missing data in the merged VIIRS SNPP/NOAA-20 ocean color product using the DINEOF method. *Remote Sensing*, *11*(2). https://doi.org/10.3390/rs11020178

Madec, G. (2011). NEMO Ocean Engine: version 3.3, (27), 1–332. Retrieved from http://www.nemo-ocean.eu/About-NEMO/Reference-manuals%5Cnpapers2://publication/uuid/73E7FF17-99BE-4B10-A823-0037C823EF6E

Martin, A. P., & Pondaven, P. (2003). On estimates for the vertical nitrate flux due to eddy pumping. *Journal of Geophysical Research: Oceans*, *108*(11), 1–10. https://doi.org/10.1029/2003jc001841

Mason, E., Pascual, A., & McWilliams, J. C. (2014). A New Sea Surface Height – Based Code for Oceanic Mesoscale Eddy Tracking. *Journal of Atmospheric and Oceanic Technology*, *31*, 1181–1188. https://doi.org/10.1175/JTECH-D-14-00019.1

Maturi, E., Harris, A., Mittaz, J., Sapper, J., Wick, G., Zhu, X., et al. (2017). A new high-resolution sea surface temperature blended analysis. *Bulletin of the American Meteorological Society*, *98*(5), 1015–1026. https://doi.org/10.1175/BAMS-D-15-00002.1

McGillicuddy, D. J., Robinson, A. R., Siegel, D. A., Jannasch, H. W., Johnson, R., Dickey, T. D., et al. (1998). McGuillicuddy_1998.pdf. *Nature*, *394*, 263–266. https://doi.org/https://doi.org/10.1038/28367

McGillicuddy, D. J. (2016). *Mechanisms of Physical-Biological-Biogeochemical Interaction at the Oceanic Mesoscale*. *Annual Review of Marine Science* (Vol. 8). https://doi.org/10.1146/annurev-marine-010814-015606

Momin, I. M., Mitra, A. K., Mahapatra, D. K., Rajagopal, E. N., & Harenduprakash, L. (2013). Indian Ocean simulation results from NEMO global ocean model. *Indian Journal of Marine Sciences*, *42*, 425–430.

Morrison, A. K., Saenko, O. A., Hogg, A. M. C., & Spence, P. (2013). The role of vertical eddy

flux in Southern Ocean heat uptake. *Geophysical Research Letters*, *40*(20), 5445–5450. https://doi.org/10.1002/2013GL057706

Nagai, T., Gruber, N., Frenzel, H., Lachkar, Z., McWilliams, J. C., & Plattner, G. K. (2015). Dominant role of eddies and filaments in the offshore transport of carbon and nutrients in the California Current System. *Journal of Geophysical Research: Oceans*. https://doi.org/10.1002/2015JC010889

Neema, C. P., Hareeshkumar, P. V., & Babu, C. A. (2012). Characteristics of Arabian Sea mini warm pool and Indian summer monsoon. *Climate Dynamics*, *38*(9–10), 2073–2087. https://doi.org/10.1007/s00382-011-1166-2

Ning, J., Chen, K., & Gaube, P. (2021). Diverse Variability of Surface Chlorophyll During the Evolution of Gulf Stream Rings. *Geophysical Research Letters*, *48*(5). https://doi.org/10.1029/2020GL091461

Park, J. E., Park, K. A., Kang, C. K., & Park, Y. J. (2020). Short-Term Response of Chlorophyll-a Concentration to Change in Sea Surface Wind Field over Mesoscale Eddy. *Estuaries and Coasts*, *43*(3), 646–660. https://doi.org/10.1007/s12237-019-00643-w

Patnaik, K. V. K. R. K., Maneesha, K., Sadhuram, Y., Prasad, K. V. S. R., Ramana Murty, T. V., & Brahmananda Rao, V. (2014). East India Coastal Current induced eddies and their interaction with tropical storms over Bay of Bengal. *Journal of Operational Oceanography*, *7*(1), 58–68. https://doi.org/10.1080/1755876X.2014.11020153

Pegliasco, C., Chaigneau, A., & Morrow, R. (2015). Main eddy vertical structures observed in the four major Eastern Boundary Upwelling Systems. *Journal of Geophysical Research: Oceans*, *120*(9), 6008–6033. https://doi.org/10.1002/2015JC010950

Prakash, K. R., Nigam, T., Pant, V., & Chandra, N. (2021). On the interaction of mesoscale eddies and a tropical cyclone in the Bay of Bengal. *Natural Hazards*, *106*(3), 1981–2001. https://doi.org/10.1007/s11069-021-04524-z

Roman-Stork, H. L., Subrahmanyam, B., & Trott, C. B. (2019). Mesoscale eddy variability and its linkage to deep convection over the Bay of Bengal using satellite altimetric observations. *Advances in Space Research*. https://doi.org/10.1016/j.asr.2019.09.054

Roman-Stork, H. L., Subrahmanyam, B., & Murty, V. S. N. (2019). Quasi-biweekly oscillations in the Bay of Bengal in observations and model simulations. *Deep-Sea Research Part II: Topical Studies in Oceanography*, *168*(June), 104609. https://doi.org/10.1016/j.dsr2.2019.06.017

Roman-Stork, H. L., Subrahmanyam, B., & Murty, V. S. N. (2020). The Role of Salinity in the Southeastern Arabian Sea in Determining Monsoon Onset and Strength. *Journal of Geophysical Research: Oceans*, *125*(1). https://doi.org/10.1029/2019jc015592

Sadhuram, Y., Maneesha, K., & Murty, T. V. R. (2012). Intensification of Aila (May 2009) due to a warm core eddy in the north Bay of Bengal. *Natural Hazards*, *63*(3), 1515–1525. https://doi.org/10.1007/s11069-011-9837-1

Santana, O. J., Hernández-Sosa, D., Martz, J., & Smith, R. N. (2020). Neural network training for the detection and classification of oceanic mesoscale eddies. *Remote Sensing*, *12*(16), 1–21. https://doi.org/10.3390/RS12162625

Scharroo, R., Leuliette, E., Lillibridge, J., Byrne, D., Naeije, M., Mitchum, G., et al. (2013). RADS : CONSISTENT MULTI-MISSION PRODUCTS, (February), 5–8.

Shankar, D., Vinayachandran, P. N., & Unnikrishnan, A. S. (2002). The monsoon currents in the north Indian Ocean. *Progress in Oceanography*, *52*(1), 63–120. https://doi.org/10.1016/S0079-6611(02)00024-1

Shenoi, S. S. C., Shankar, D., & Shetye, S. R. (1999). On the sea surface temperature high in the Lakshadweep Sea before the onset of the southwest monsoon. *Journal of Geophysical Research: Oceans*, *104*(C7), 15703–15712. https://doi.org/10.1029/1998jc900080

Su, Z., Wang, J., Klein, P., Thompson, A. F., & Menemenlis, D. (2018). Ocean submesoscales as a key component of the global heat budget. *Nature Communications*, *9*(1), 1–8. https://doi.org/10.1038/s41467-018-02983-w

du Toit, P. C., & Marsden, J. E. (2010). Horseshoes in hurricanes. *Journal of Fixed Point Theory and Applications*, *7*(2), 351–384. https://doi.org/10.1007/s11784-010-0028-6

Trott, C. B., Subrahmanyam, B., Chaigneau, A., & Roman-Stork, H. L. (2019). Eddy-induced Temperature and Salinity Variability in the Arabian Sea. *Geophysical Research Letters*, *46*(5), 2734–2742. https://doi.org/10.1029/2018GL081605

Twining, B. S., Nuñez-Milland, D., Vogt, S., Johnson, R. S., & Sedwick, P. N. (2010). Variations in Synechococcus cell quotas of phosphorus, sulfur, manganese, iron, nickel, and zinc within mesoscale eddies in the Sargasso Sea. *Limnology and Oceanography*, *55*(2), 492–506. https://doi.org/10.4319/lo.2009.55.2.0492

Woodworth, P. A., Schorr, G. S., Baird, R. W., & Webster, D. L. (2011). Lincoln Eddies as offshore foraging grounds for melon-headed whales (Peponocephala electra). *Marine Mammal Science*.

Xiu, P., Palacz, A. P., Chai, F., Roy, E. G., & Wells, M. L. (2011). Iron flux induced by Haida eddies in the Gulf of Alaska. *Geophysical Research Letters*, *38*(13), 1–5. https://doi.org/10.1029/2011GL047946

Yi, J., Du, Y., He, Z., & Zhou, C. (2014). Enhancing the accuracy of automatic eddy detection and the capability of recognizing the multi-core structures from maps of sea level anomaly. *Ocean Science*, *10*(1), 39–48. https://doi.org/10.5194/os-10-39-2014

Zhang, S., Curchitser, E. N., Kang, D., Stock, C. A., & Dussin, R. (2018). Impacts of Mesoscale Eddies on the Vertical Nitrate Flux in the Gulf Stream Region. *Journal of Geophysical Research: Oceans*, *123*(1), 497–513. https://doi.org/10.1002/2017JC013402

Zhang, Y., Hu, C., Liu, Y., Weisberg, R. H., & Kourafalou, V. H. (2019). Submesoscale and Mesoscale Eddies in the Florida Straits: Observations from Satellite Ocean Color Measurements. *Geophysical Research Letters*, *46*(22), 13262–13270. https://doi.org/10.1029/2019GL083999